Wind Stress on the Tropical Oceans during the Year of FGGE

A REPORT

from the space science and engineering center
the university of wisconsin-madison
madison, wisconsin

Wind Stress on the Tropical Oceans

during the Year of FGGE

A Report to

The National Science Foundation

for

Grant ATM-81-19895

University of Wisconsin Account 144 R041

V. E. Suomi, Principal Investigator

Final Technical Report

by Donald P. Wylie
Barry B. Hinton
and
Michael R. Howland

The Space Science and Engineering Center
University of Wisconsin-Madison
Madison, Wisconsin 53706

October 1984

Published by
The University of Wisconsin-Madison
Space Science and Engineering Center
1225 West Dayton Street
Madison, Wisconsin 53706

Reproduced in the United States of America
ISBN 0-000-00000-0

This work is a result of research sponsored by NSF, the National Science Foundation, under Grant Number ATM-81 19895. The U.S. Government is authorized to produce and distribute reprints for governmental purposes notwithstanding any copyright notation that may appear hereon.

Contents

Preface

A requirement for sea-surface stress appeared in almost every program-planning document in the decade leading up to the 1979 Global Weather Experiment (NAS, 1969; ICAS, 1977; NASA, 1980). The work described in this report was undertaken as soon as it became evident that microwave scatterometer data expected from Seasat-A would not be available. Initially, we confined our attention to the Summer Monsoon study area in the Indian Ocean. This was sponsored by the National Science Foundation under Grant ATM-79-13097 and is described in our final report dated 20 February 1982. Under Grant ATM-81-19895, the work has been extended to the entire marine low-latitude zone. As part of this process, the Indian Ocean work has been updated. In this Final Report for ATM-81-19895, we summarize some of the important results of this effort. More complete results are available to other investigators on computer-compatible tape. The experience gained has already had an important influence on planning of future programs, WOCE and TOGA.

Wind Stress on the Tropical Oceans during the Year of FGGE

Part I. Method

1. Introduction

The First GARP Global Experiment (FGGE, also called the Global Weather Experiment, Fein and Kuettner 1980) produced many cloud motion observations to supplement conventional wind observations of the World Meteorological Organization (WMO) network. We have combined one full year of intensive observations (from December 1978 through November 1979) with the merchant ship data to form composite surface wind and wind stress analyses for the zone within ±20° of the equator. This is an expansion of the Indian Ocean analyses made by Wylie and Hinton (1982a). It is one of the few contemporary global scale wind data sets derived purely from "real data" (i.e., without the influence of numerical models).

Sections 2-6 of Part I describe the methods used to produce the wind analyses. In Appendix A, we compare wind and stress patterns for the FGGE year (shown by our charts in Part 2) to three climatologies. These are the Hastenrath and Lamb atlases of the Indian (1979), the tropical Atlantic, and eastern Pacific Oceans (1977); the global wind climatology of Hellerman and Rosenstein (1983); and the regional climatology of the Somali Jet in the Indian Ocean made by Bruce (1978). The departures of the FGGE year from Hastenrath and Lamb will be discussed month-by-month in Section A.2. Comments on Hellerman and Rosenstein will be included in the January and July discussions of the same section. The oscillation of the Arabian Sea and trade winds is discussed in Section A.3. Comparisons to past monsoons described by Bruce (1978) and Fieux and Stommel (1977) are made in Section A.4.

2. Cloud Motion Data

Cloud motions were analyzed from the images of five geostationary satellites around the world (see Table 1). The western hemisphere was covered by the National Atmospheric and Oceanic Administration National Environmental Satellite Services (NOAA/NESS) and the University of Wisconsin, using the Geostationary Operational Environmental Satellites (GOES). Cloud motions were obtained over parts of the Atlantic and Pacific Oceans from 20°W to 180°W. The NOAA/NESS observations spanned to ±50° latitude, while the University of Wisconsin augmented the coverage in the tropics from 15°N to 15°S, using the same GOES satellites. The western Pacific was covered by the Japanese Geostationary Meteorological Satellite (GMS), from 100°E to 180°E longitude. The University of Wisconsin augmented these data from 50°N to 50°S for five months during the special observing periods of FGGE (December-February and May-June, 1979). The Indian Ocean was covered from the African continent to 100°E longitude by a third GOES satellite of the United States. Cloud motions were measured by the University of Wisconsin from 30°N to 40°S latitude. Additional data in the western Indian Ocean and eastern Atlantic were obtained from the European Space Agency (ESA) using Meteosat, the fifth geostationary satellite.

Cloud motions were measured by a variety of methods (Mosher, 1981). Most institutions used statistical correlations over small target areas on the images to measure cloud displacements from one time to the next, usually two images one-half hour apart. Two sequential measurements usually were made over three images in a one-hour time span for consistency quality control checks. The two measurements were averaged together if they agreed within 5 m/s for each wind component. Otherwise, they were discarded by the quality control algorithm.

The cloud targets were manually selected by meteorologists viewing the satellite images at the Japanese Meteorological Satellite Center (JMSC) and Wisconsin, while NOAA/NESS and ESSA used automatic methods attempting to extract motions at regularly spaced intervals on the satellite images. The manual selection methods also provided a first guess of the cloud target's motion to aid the target tracking algorithms.

Table 1: Summary of the sources of cloud motions used in the analysis.

Data Producing Institution	Satellite	Longitude Bounds	Latitude Bounds	Time Period
U.S. NOAA/NESS	GOES-East	20°W-110°W	50°N-50°S	1 Dec 78-30 Nov 79
	GOES-West	90°W-180°W	50°N-50°S	same
Univ. Wisconsin	GOES-East	20°W-110°W	15°N-15°S	same
	GOES-West	90°W-180°W	15°N-15°S	same
	Indian Ocean GOES	20°E-100°E	30°N-40°S	same
Japanese Meteorological Satellite Center	GMS	90°E-180°E	40°N-40°S	same
Univ. Wisconsin	GMS	90°E-180°E	40°N-40°S	1 Jan 79-28 Feb 79 1 May 79-30 Jul 79
European Space Agency	Meteosat	40°W-40°E	50°N-50°S	1 Dec 78-30 Nov 79

The quality of wind fields described by cloud motions depends on two factors: 1) the accurate alignment of the time sequence of geostationary satellite images, and 2) the density of motion observations that can be extracted from the images. Cross comparisons between cloud motions measured by different institutions in areas of overlapping coverage found no significant biases (Mosher 1981). This indicated that the image registration or navigation procedures used by the various institutions

produced similar results. Mosher (1981) states that image registration or alignment errors caused less than 2 m/s bias errors.

Comparisons between neighboring observations from the same producer indicate that random errors were less than 3 m/s (Mosher 1981, Wylie and Hinton 1982b, and Wylie et al. 1984). Changes in the cloud targets over the tracking time interval and the vertical wind shear were the main causes of the random errors.

All "low level" cloud motions were used in this analysis. Heights of the cloud motion vectors were sometimes estimated from the infrared temperatures on satellite images, and sometimes assigned to one fixed level. Each data producer had a specific preference for height assignment methods. ESA used the coldest infrared temperature of the cloud target which normally corresponds to the cloud top. But detailed studies by Hasler et al. (1979) found that low level clouds usually move with speeds of their bases rather than their tops. Comparisons of satellite derived cloud motions to radiosonde winds by Hubert and Whitney (1979) and Lee (1980) found the best correlations to be with 900 mb winds which were near the cloud base level. NOAA/NESS assigned all low level cloud motions to 900 mb. Wisconsin followed a similar procedure for part of their data, while using a more complicated scheme for estimating cloud base for most of their data. Both Wisconsin and JMSC estimated cloud base heights using the coldest infrared temperature of the cloud top and an estimation of cloud thickness.

These above methods resulted in low level clouds being assigned various heights from 700 to 950 mb. Since all were intended to indicate low cumulus clouds with boundary layer roots, we have generally used cloud motions between 700 mb and the surface in our analysis. Wisconsin data was

an exception. By convention 700 mb assignments sometimes indicated middle clouds above the boundary layer related clouds. Thus, we restricted the Wisconsin winds in this study to those below 800 mb.

The cloud motion observations closest to local noon on each day were used. This gave preference to techniques that used visible satellite images and ignored some data sets where only infrared images were used. Wisconsin tracked clouds at 18GMT for GOES-E, 20GMT for GOES-W, and 09GMT for the Indian Ocean. These data sets presented numerous targets since small low level clouds and cloud groups are easier to identify on the visible images than the infrared. NOAA/NESS provided data sets at three times per day, usually from infrared images alone. We used only the 18GMT data to be consistent with the Wisconsin data. We obtained one GMS data set produced by JMSC near 00GMT for each day. A supplementary data set from GMS produced by Wisconsin for the five months of the special observing periods was obtained between 23 and 00GMT. We used the 12GMT data set from ESA. Data sets at other times were ignored.

3. Method of Analysis

The low level cloud motion measurements were analyzed on uniform grids of 2° latitude by 4° longitude spacing, from 20°N to 20°S latitude and 0°E to 360°E longitude. The analysis procedure described in Wylie and Hinton (1982a) was applied on a daily basis. Grid point values were determined from the weighted sum of cloud motion measurements within 6° of latitude and longitude of each grid point. Grid points with less than two cloud motion measurements within this distance were not filled but were marked as having no cloud data for that day. The weighting function, W, is defined by (1).

$$W = 4./(4. + R^2), \quad (1)$$

R is the distance in degrees latitude and longitude from each grid point. This weighting function approximated a Gaussian low pass filter. Special exceptions were made in the eastern Pacific, the South China and adjacent seas (100° to 130°E), and the Mascarene Channel in the Indian Ocean where search distance (R) was restricted to 2° because of high variability in those areas. This will be discussed further in Section 4.

The data were edited for spurious or deviant observations. Cloud motions that differed by more than 5 m/s in either the U or V component from the weighted mean at each grid point were rejected, and the mean recomputed.

Ship data were also corrected for biases at low speeds. Under light winds the errors in the speed estimates will be biasd high. This is a result of observers not being able to estimate negative wind speeds. The unsymmetrical nature of the speed estimates around the true wind implies that the mean of several ship observations will be larger than the true wind when speeds are below 7 m/s. This can be shown by modelling the distribution of wind reports, using a probability function and truncating the negative values from the distribution. The truncation will raise the mean. We corrected the ship wind analysis grid speed (S_c) from the distance weighted average of the observations (S_o), using an exponential function.

$$S_c = S_o - 1.99 \text{ EXP } (-0.41\ S_o) \quad (2)$$

This function approximates the theoretically derived correction, which was tested in comparisons of ship and NOAA data buoy observations.

4. Combination with Ship Data

The cloud motion gridded analyses were converted to estimates of the surface wind, using a statistical boundary layer which was developed by comparing the cloud motions to all available ship reports. Ship reports were obtained from the FGGE Level IIb and the supplemental marine data archives processed by the Mobile Ship Data Center in Hamburg, F.R.G.

The statistical boundary layer consists of wind component corrections made to the cloud motion gridded analyses. After thorough study, these corrections were developed separately for four different seasons and 16 geographical regions (see Figure 1). The ship wind reports were separately analyzed on 2°x4° grids, using the same procedure as the cloud motions. All ship reports during the day, 00GMT to 23GMT, were aggregated and subjected to the same editing procedure. Air-sea temperature differences were analyzed on the same grids, using the ship reported temperature data.

Empirical regressions were used to link these surface level wind components (U_s and V_s) to the cloud level motion components (U_c and V_c), air-sea virtual temperature difference (T_{a-s}), and the coriolis parameter (f) for the latitude of the grid point.

$$U_s \text{ or } V_s = C_0 + C_1 U_c + C_2 V_c + C_3 T_{a-s} + C_4 f \qquad (3)$$

A linear multiple regression was derived for each surface wind component in each partitioned area (Fig. 1), using a statistical analysis package, SPSS (Hull and Nie 1981). The gridded cloud motions were used for the observed values of U_c and V_c and gridded ship data for observed values of U_s, V_s, and T_{a-s} within each area and season to derive the empirical relationships. Because of the length of the resulting table, the coefficients for (3) are given in Appendix B.

Only parameters that have high correlations with the surface (ship) winds were used in the equations. The decision to reject parameters was made objectively by the SPSS software. Usually the U_c was a significant predictor for U_s, and the V_c a significant predictor for V_s (See Fig. 2). The others, f and T_{s-a}, were used in some but not all areas. This does not mean that f and T_{s-a} are physically unimportant globally. Our study area encompasses low latitudes where one would expect f to be less important. The range of T_{s-a} values in some regions is small or does not span a transition in stability.

In the original formulation of this algorithm for transforming cloud motion winds to the surface level, we considered longitude as an additional variable. Smaller boxes also were tested. However, little longitudinal variation was found in the empirical relationships across the major ocean basins, so we simplified our algorithm using fewer boxes spanning large longitudinal sectors. Smaller boxes proved necessary in areas where variable winds or variable cloud-ship shears were found. These were near coastal influences such as the eastern Pacific (Boxes 2 and 6) and the Mascarene Channel (Box 16).

The cloud motion grids were converted to surface level winds, using (3) with the coefficients listed in Appendix B. On the boundaries of the boxes the empirical relationships were averaged to blend continuously from one box to another. The averaging was applied to two rows or columns of grid points together, since the box boundaries were located between the grid points. In boxes and seasons where SPSS did not derive a coefficient for relating corresponding cloud and ship wind components, the surface grid point was not filled with cloud-derived values. That is, if U_s proved independent of U_c or V_s proved independent of V_c, we inferred that cloud

motions and surface motions were locally uncoupled and one should not attempt to calculate (U_s,V_s) from (U_c,V_c). This will be discussed further below.

Figure 3 illustrates the typical effects of the statistical boundary layer. The upper panel shows the annual mean ratio of ship-to-cloud speed predicted by the regression relations. As one would expect, these ratios are from 0.70 to 0.95. The lower panel shows the mean regression predicted veering, or directional difference between cloud level and the surface. Regions of southerly mean flow south of the ITCZ exhibit backing (negative veering) largely in the range -7° to -28°. North of the ITCZ veering from 9° to 18° dominates.

The final step of the daily cloud-ship analysis was the combination of the cloud motion grid, now corrected for subcloud shear, with the ship analysis grid. To merge the two candidates, we chose an arbitrary weighting function.

$$W_c = 2/(2 + N_s) \tag{4}$$

The weight, W_c, given to the surface corrected cloud grid was calculated from the number of ship observations (N_s) used in the ship grid at each grid point. The ship grid was given the complementary weight W_s.

$$W_s = 1 - W_c. \tag{5}$$

Therefore, where two ships were present for a grid point, each grid was given equal weighting ($W_s = W_c = 0.5$). Where four ships were present, the ship grid clearly dominated ($W_s = 0.67$, $W_c = 0.33$). This method allowed the ship grid to dominate where many observations were available and smoothly blended into the cloud grid outside the ship tracks.

Not all grid points were filled on each daily grid. Recall that search radius and editing criteria were applied separately to the cloud

data and the ship data as described in Section 3. If a cloud motion grid value and corresponding ship grid value were both missing, no combination grid was possible. The sub-cloud shear correction also had to be a straightforward relationship for each wind component as mentioned above. Otherwise, the cloud grid point was not transformed to the surface.

This method may appear complicated, but its rudiments are simple. It depends on the existence of both cloud and ship data, so that gridded analyses can be produced and empirical relationships for correcting cloud motions for subcloud shear can be built. The subcloud shear corrections are flexible, changing in a continuous manner for different wind regimes and following known properties of boundary layer dynamics. The corrected surface wind speeds are a fraction of the cloud wind speeds, with small modifications due to thermal stability (T_{s-a}) and coriolis acceleration (f).

As mentioned previously, in some areas (boxes) during some seasons, the cloud motions were <u>not</u> transformed to the surface because the transfer relationships were unrealistic or could not be formed because of the lack of data. In the eastern Pacific (Boxes 2 and 6 in Figure 1), the cloud data were ignored during the fall season because the transfer algorithms were unrealistic. We felt that the wind components should be derived from the corresponding cloud components. That is, U_s should be derived at least partly from U_c ($C_1 \neq 0$) and V_s from V_c ($C_2 \neq 0$). Where the SPSS software rejected the corresponding cloud wind component, we felt the empirical relationship was unrealistic. The seasons and boxes where these problems occurred are marked in Appendix B.

Box 6 in the eastern Pacific (±5° latitude east of 90°E) had all of the problems mentioned above in all seasons. Consequently, surface wind

products for this area contain only ship data when present. Similar problems were found in the eastern Atlantic in Box 8 (±5° latitude, east of 15°E) for the winter, summer, and fall seasons. The South China Sea maritime continent areas in Boxes 13 and 14 (100°-140° longitude) presented problems in defining the vertical shear algorithm for the meridional (V) component in the fall, as did the Mascarene channel, Box 16. In these locations and seasons, our surface wind analysis was derived entirely from the ship wind analyses without any cloud motion information.

5. Discussion of Cloud-Ship Comparison

Correlations of ship with cloud wind components are reasonably high, 0.5-0.76 (Fig. 2). The highest correlations were the U-component, perhaps because this is the largest component over the tropical belt examined. The Arabian Sea sector of the Indian Ocean had large correlations for both U and V components. This results from the large seasonal changes of the monsoon winds in this area. The description of the monsoon is one of the strong points of this analysis. Other high correlations were found in the 100° to 140°E sector and the equatorial eastern Pacific bounding the South American coast.

The standard errors in predicting the ship wind components from the cloud winds and other variables in equation (3) are shown in Figure 4 for all 16 boxes. These error estimates (E_u and E_v) are the root mean squares of the estimated surface wind components (U_s,V_s) minus the gridded ship observation components (U_{sh},V_{sh}). For example,

$$E_u = \sqrt{\frac{1}{N}\Sigma(U_s - U_{sh})^2} \qquad (6)$$

E_u and E_v were computed daily for individual grid points and arranged in Figure 4.

The standard error estimates for daily wind analyses are reasonably small, ranging from 1.3 to 2.6 m/s. Lowest values are in equatorial regions with light winds. The errors of our wind analysis are thought to be no larger than these values. We cannot determine the expected improvement due to combining the ship with the cloud data, since we have no independent source for comparison data on a global scale.

The monthly averaged winds are expected to be more accurate than the daily values. Thirty or 31 days are averaged each month, but errors in the boundary layer correction may be correlated over several days. Halpern and Knox (1983) estimate the characteristic auto-correlation time of cloud motions to research quality buoy data to be around 5 days. This suggests that a monthly composite is formed with about 6 degrees of freedom. Thus we estimate that monthly wind fields have errors of $2.5/\sqrt{6} = 1.0$ m/s or less.

6. The Method of Estimating Wind Stress

The daily surface wind analyses were converted to estimates of the wind stress, using the bulk aerodynamic formula

$$\tau = \rho C_d U^2 \tag{7}$$

where U is the wind speed, ρ is the density of the air, and C_d is the drag coefficient. A linear variation with wind speed, as recommended by Wu (1980), was used for C_d.

$$C_d = (0.8 + 0.065\ U)\ 10^{-3}. \tag{8}$$

We obtained ρ from gridded analyses of the ship reports of air temperature.

These temperature analyses were made on the same 2°x 4° grids as the wind analyses, using the same weighting function as the wind speeds (1).

The Wu (1980) drag coefficient formula (7) was chosen from several possibilities because it is similar to other studies. Summaries and comparisons of the drag coefficient formulations can be found in Kondo (1975), Smith (1981), Bunker (1976), and Garratt (1977). The different formulae vary within ±20% of Wu (1980). The Smith (1980) formula, from data taken at Nova Scotia, is the lowest. The Bunker (1976) formula is one of the highest. Investigators agree that the drag coefficient increases with wind speed and also slightly with stability. Tropical observations such as Pond et al. (1974), in the Arabian Sea, Dunckel et al. (1974), and Businger and Seguin (1977) in the Atlantic, tend to find slightly higher drag coefficients than Smith (1980). This may be because the tropical boundary layer is usually slightly unstable. Smith (1980) used data from neutral conditions, while many of the others obtained in the tropics were presented without any stability corrections.

Bunker (1976) presents an alternative drag coefficient formula for use with monthly averaged wind fields. His formula compensates for the error that would result from averaging the winds over a month before stress computation. This is necessary because stress is roughly a function of the square of the wind speed (7), giving the higher wind events in the month more influence on the monthly average than the lower winds.

In this report we will present monthly average wind and monthly average wind stress calculated from daily analyses of the wind and daily analyses of the stress fields. In Appendix A we shall compare our results in part 2 with climatologies compiled before FGGE.

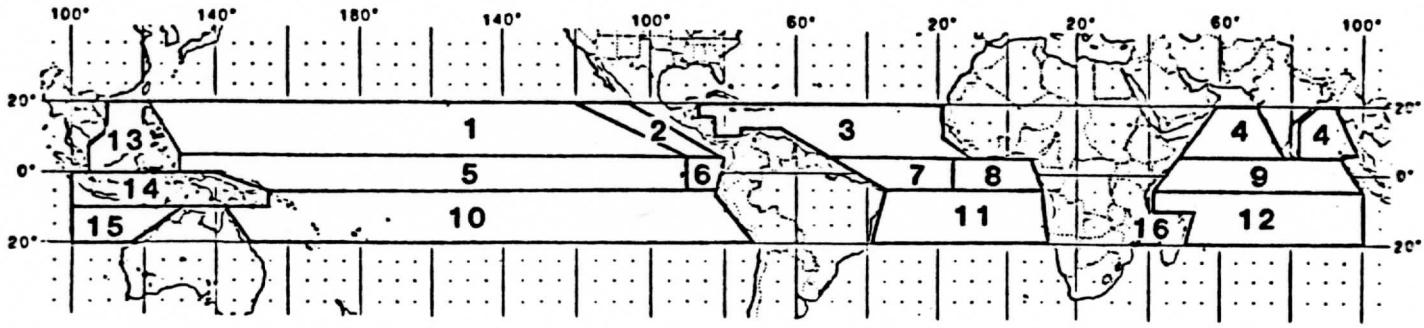

Figure 1: The locations of the boxes used for comparing cloud motions to ship reports.

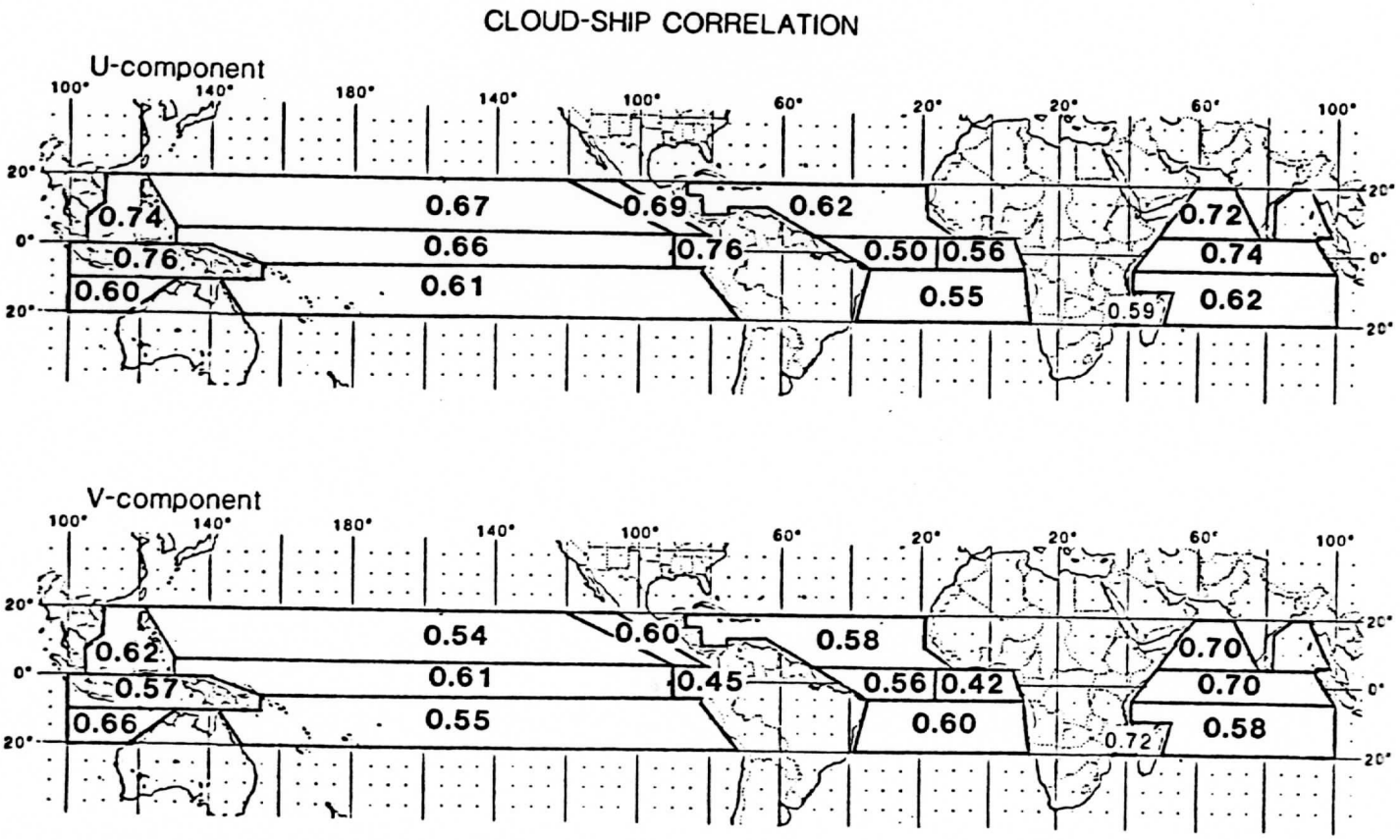

Figure 2: The correlations between cloud motions and ship winds on daily 2° lat. by 4° long. grids for the Year of FGGE. All low level cloud motions from all satellites were used in forming the daily cloud motion analyses.

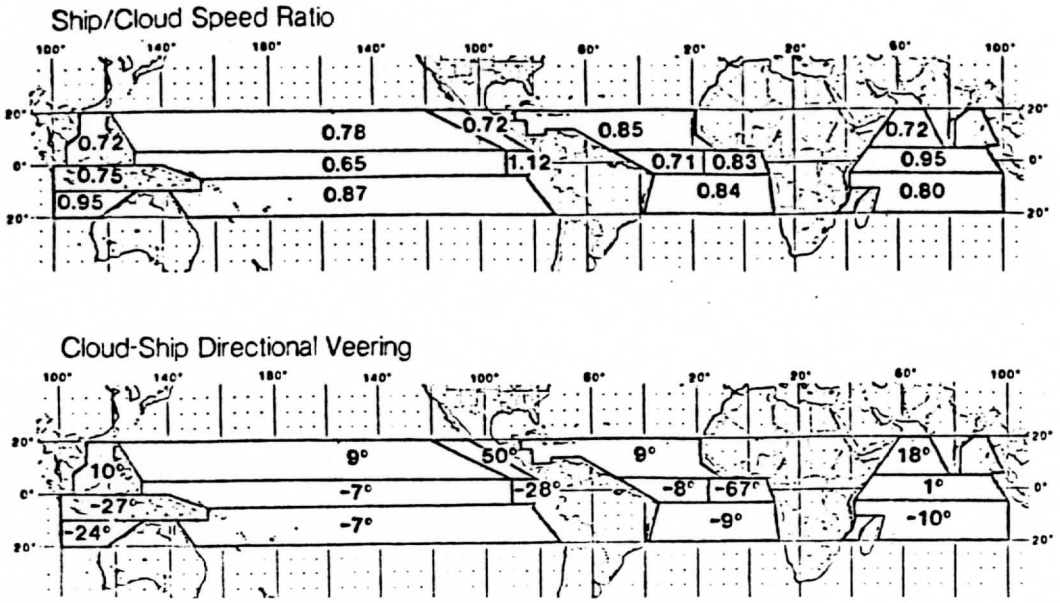

Figure 3: Average ratio of ship reported speed to cloud motion speed and average veering between cloud level and mast level for the FGGE Year.

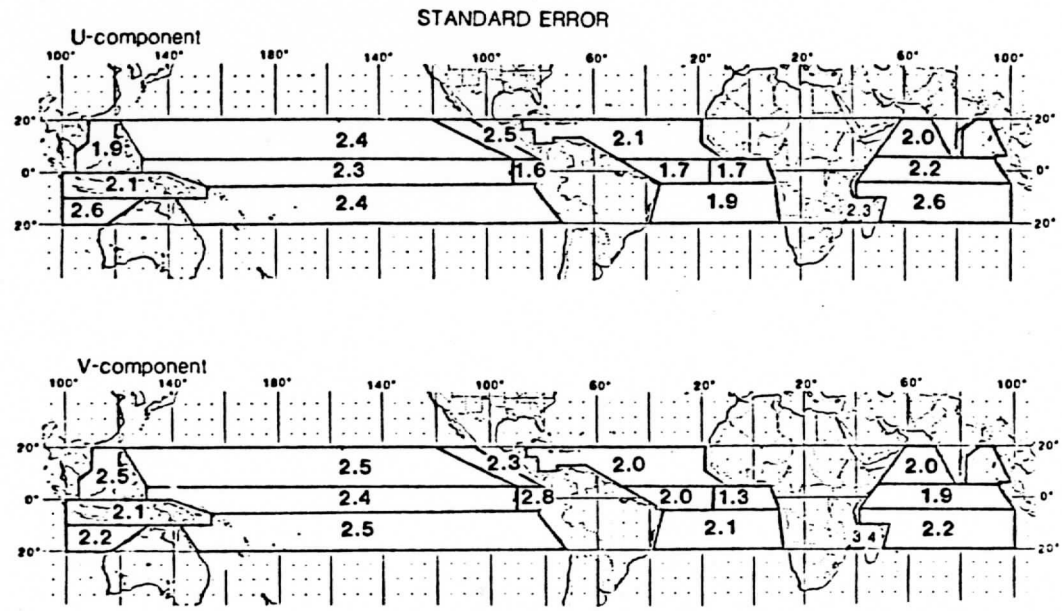

Figure 4: The standard error estimates of surface wind components estimated from cloud motions, air-sea temperature difference (ship reported), and the coriolis parameter. The standard error is the r.m.s. difference of the surface wind estimates from teh ship reports using equation (3) on a daily basis.

Wind Stress on the Tropical Oceans during the Year of FGGE

Part II. Wind and Stress Charts

Explanatory notes

The basic material developed by the methods discussed in Part 1 consist of over 700 daily wind and stress analyses. Each of these can be differentiated to yield an associated curl or divergence analysis, or groups can be aggregated to produce various time resolutions. From the vast number of possible analyses we have selected a small number for presentation here. However, the entire set is available to other investigators in the form of computer compatible tape.

Units used for wind speeds are ms^{-1}. Other quantities have a multiplier associated with the basic unit. Specifically, stress is shown in units of 10^{-2} N m^{-2} or 10^{-2} Pa; the curl and divergence of the wind are both in units of 10^{-6} S^{-1}; and curl and divergence of the stress are both in units of 10^{-8} N m^{-3} or 10^{-8} Pa m^{-1}.

Chart 1

STRESS DEC 1978

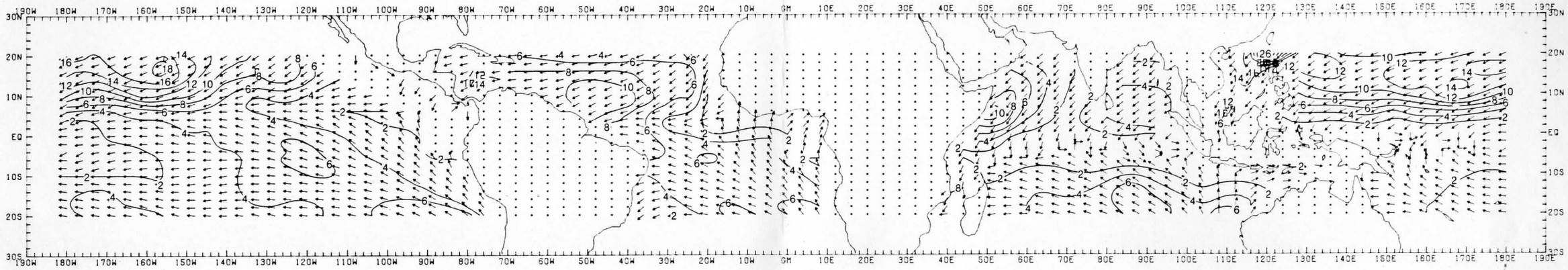

STRESS JAN 1979

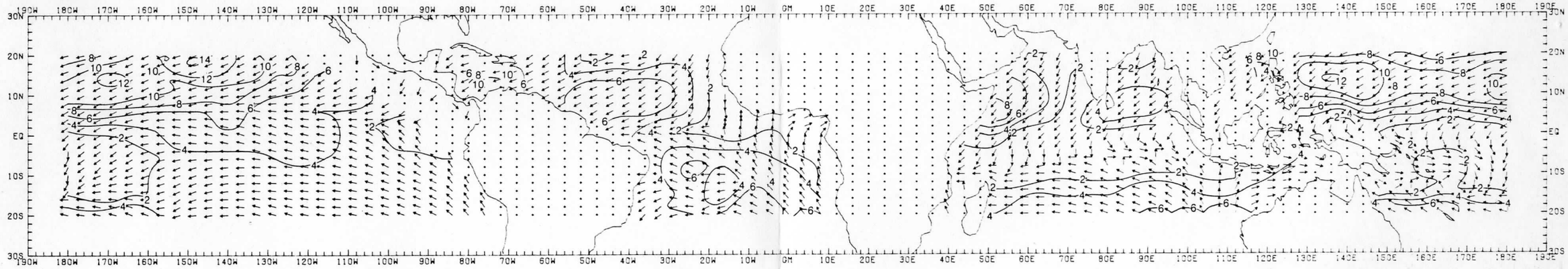

STRESS FEB 1979

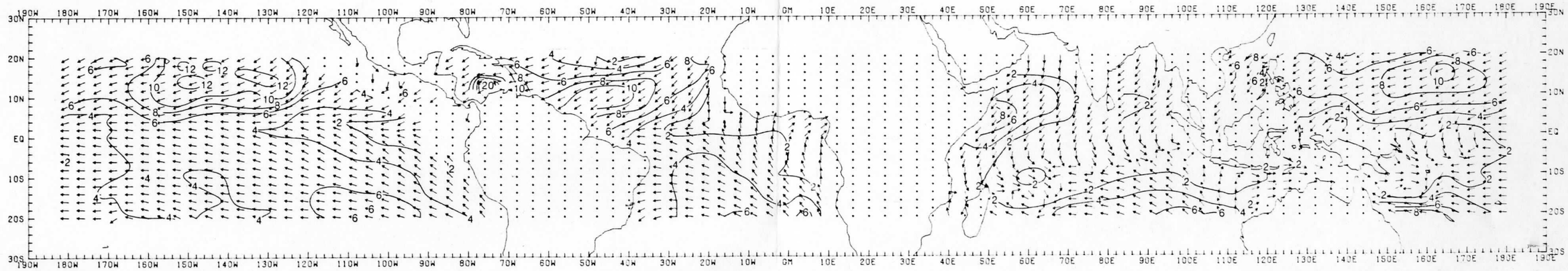

STRESS MAR 1979

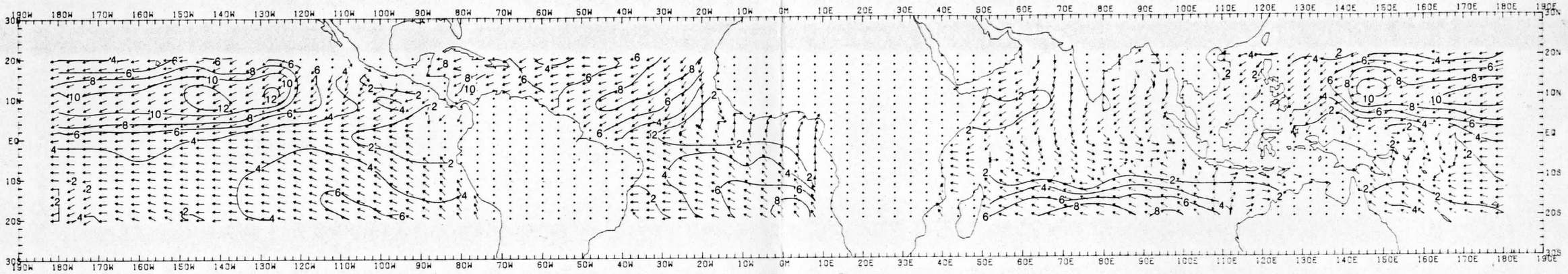

STRESS APR 1979

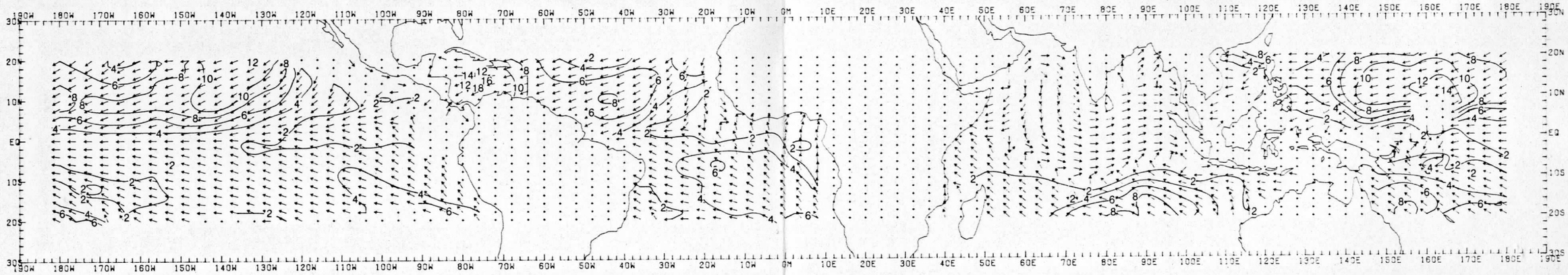

STRESS MAY 1979

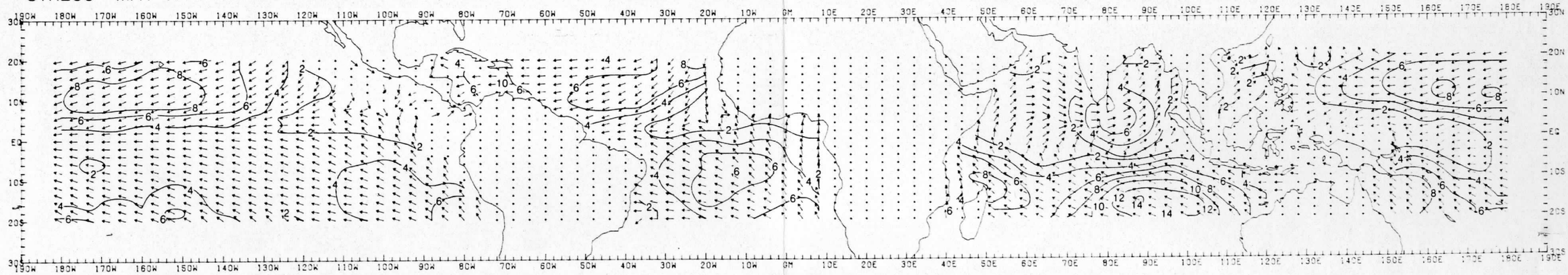

STRESS JUN 1979

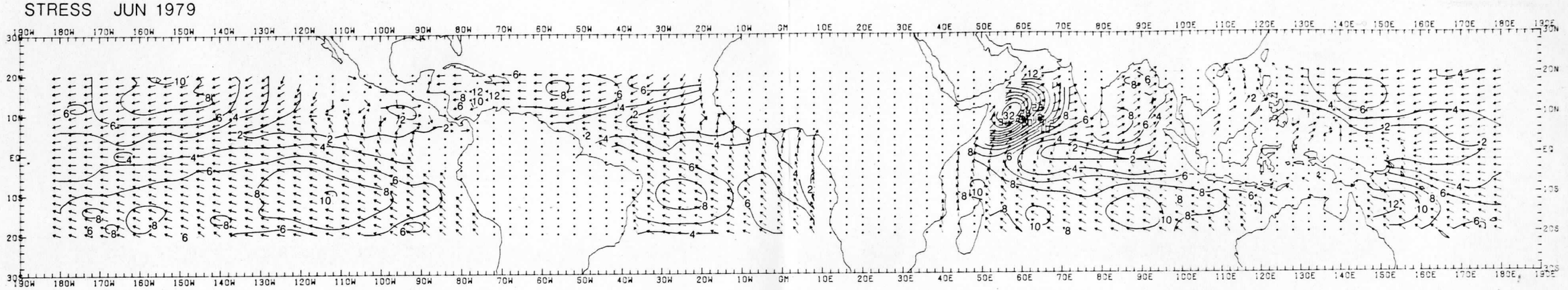

STRESS JUL 1979

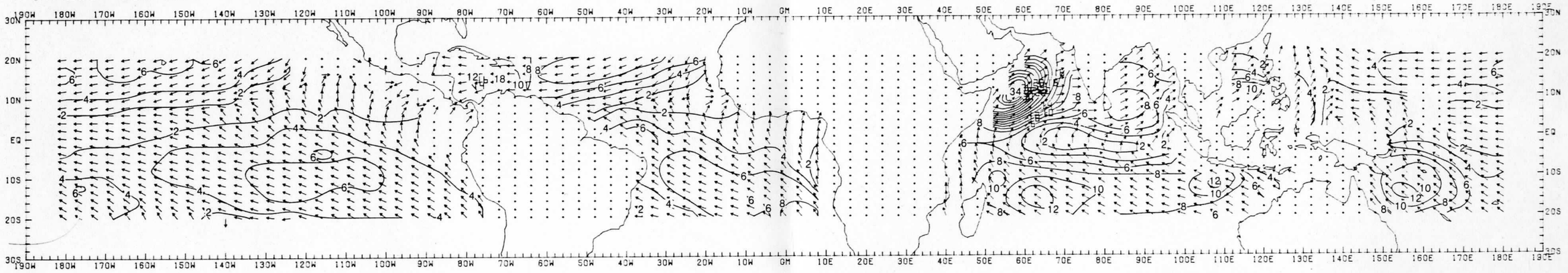

STRESS AUG 1979

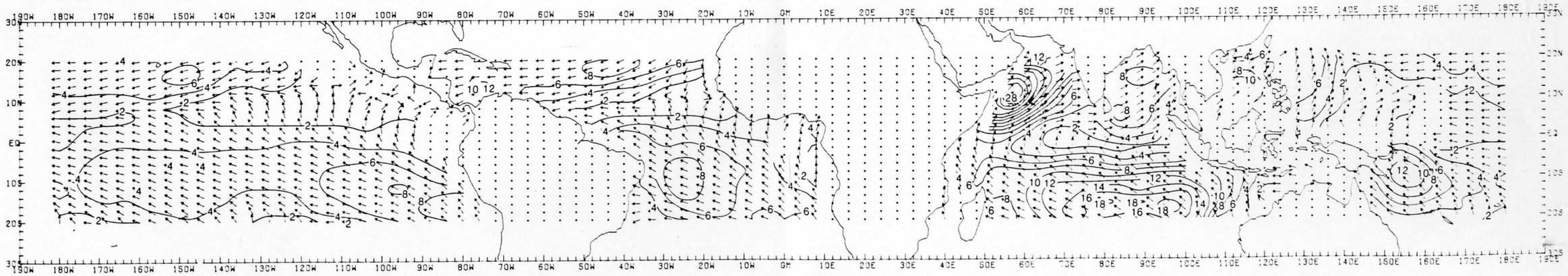

STRESS SEP 1979

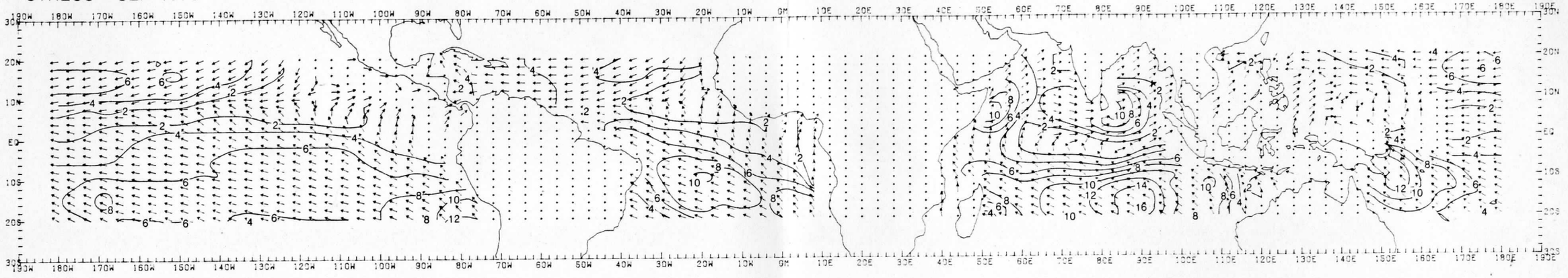

STRESS OCT 1979

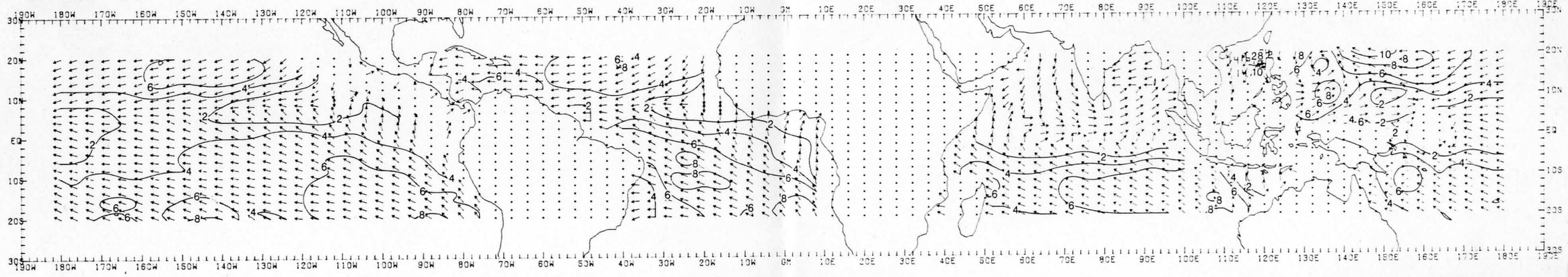

STRESS NOV 1979

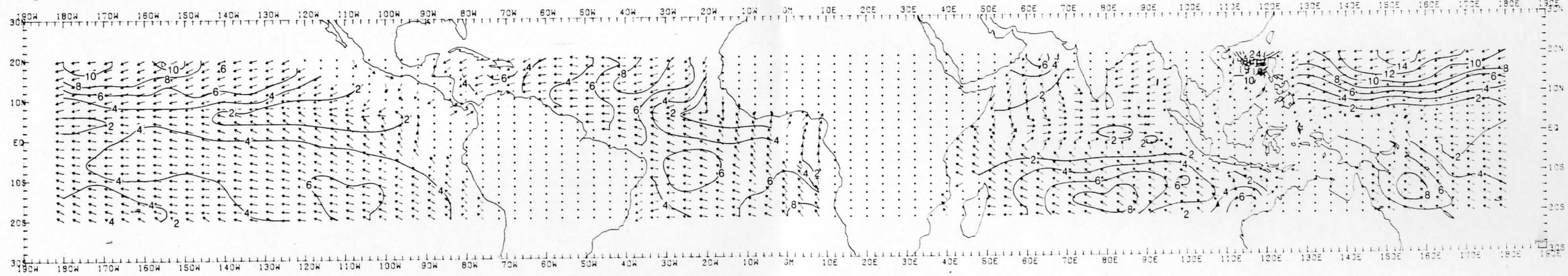

WIND JAN 1979

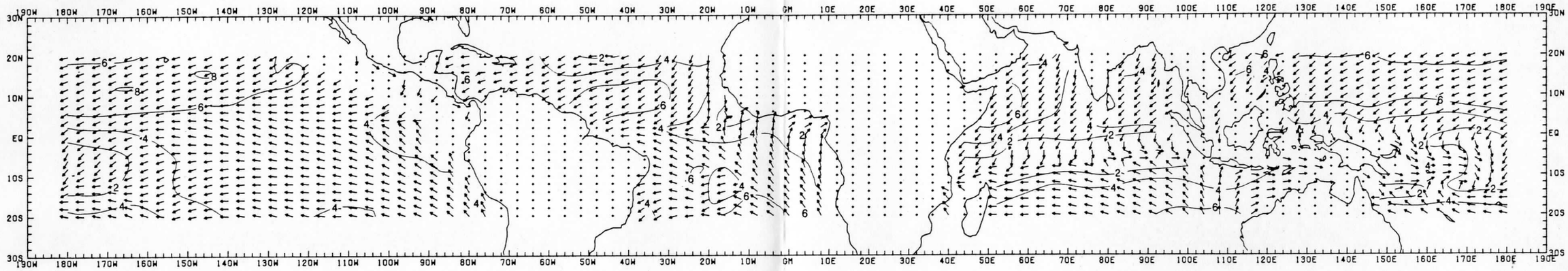

DIVERGENCE JAN 1979

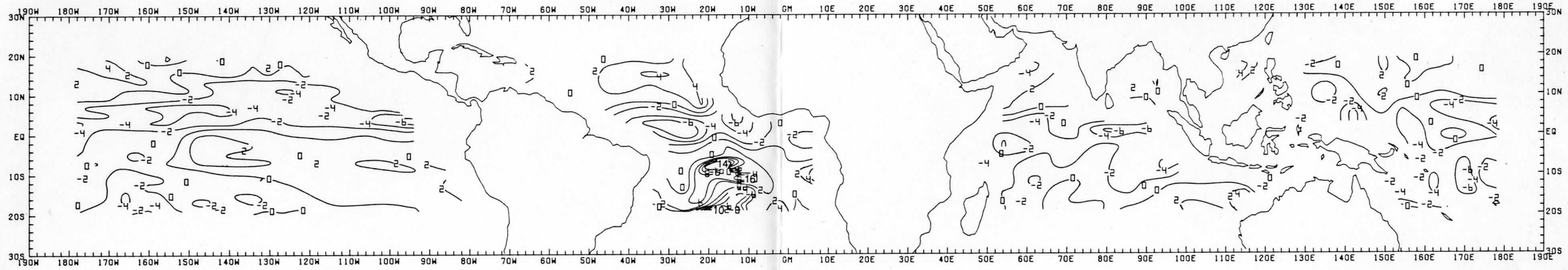

VORTICITY JAN 1979

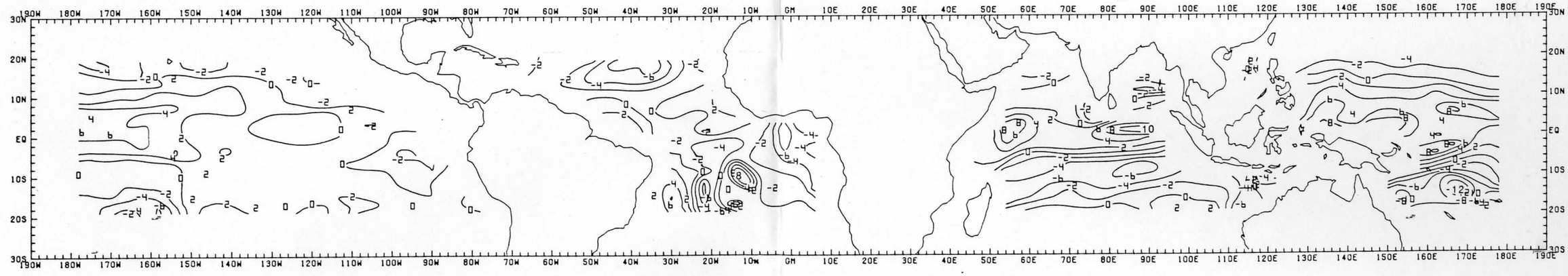

WIND APR 1979

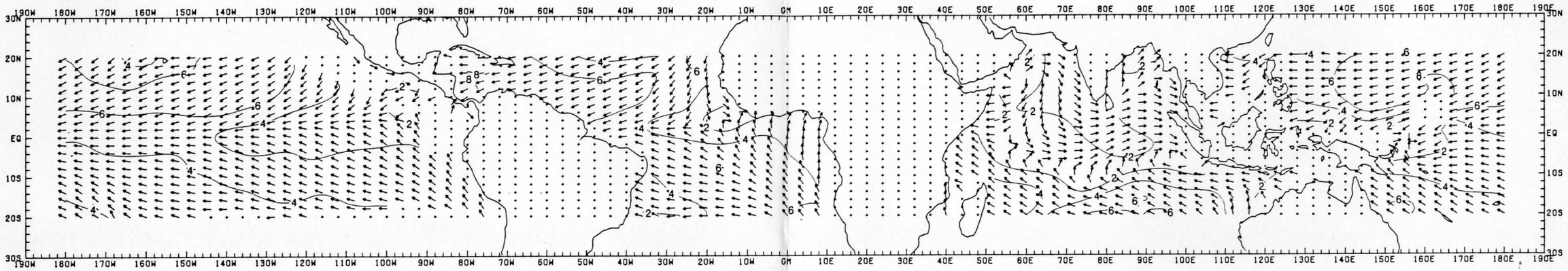

DIVERGENCE APR 1979

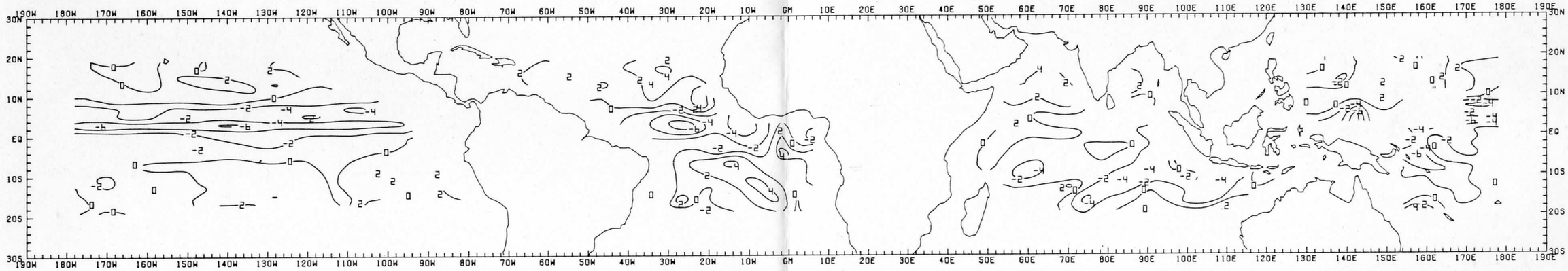

VORTICITY APR 1979

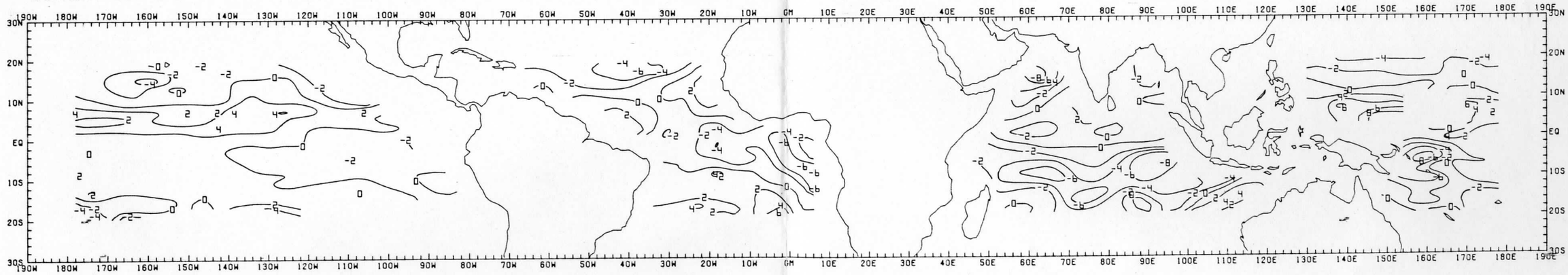

WIND JUL 1979

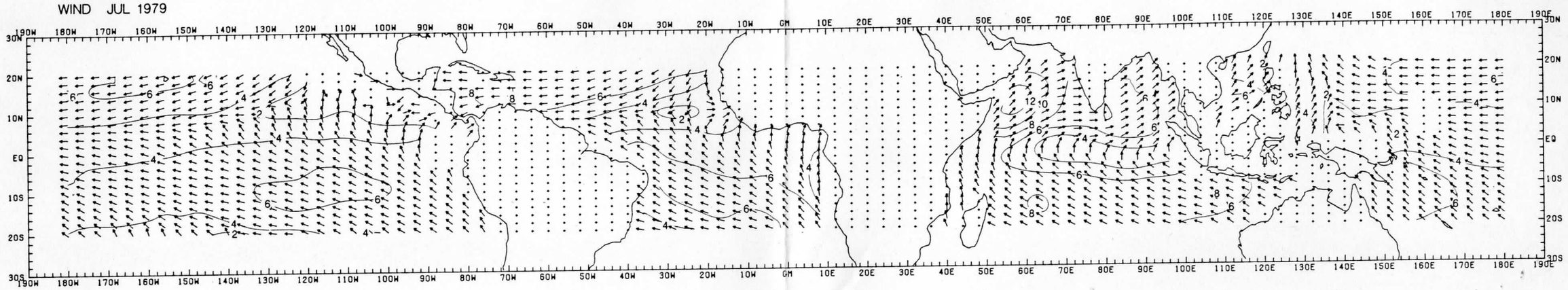

DIVERGENCE JUL 1979

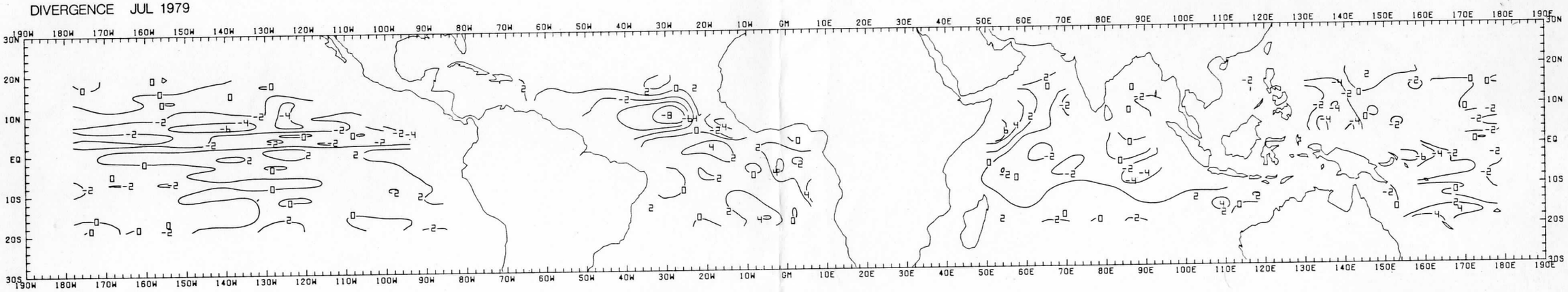

VORTICITY JUL 1979

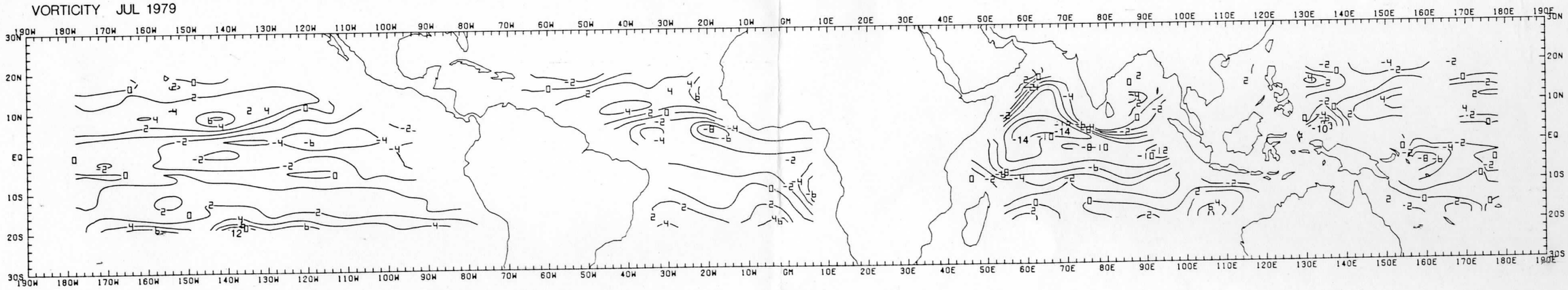

WIND OCT 1979

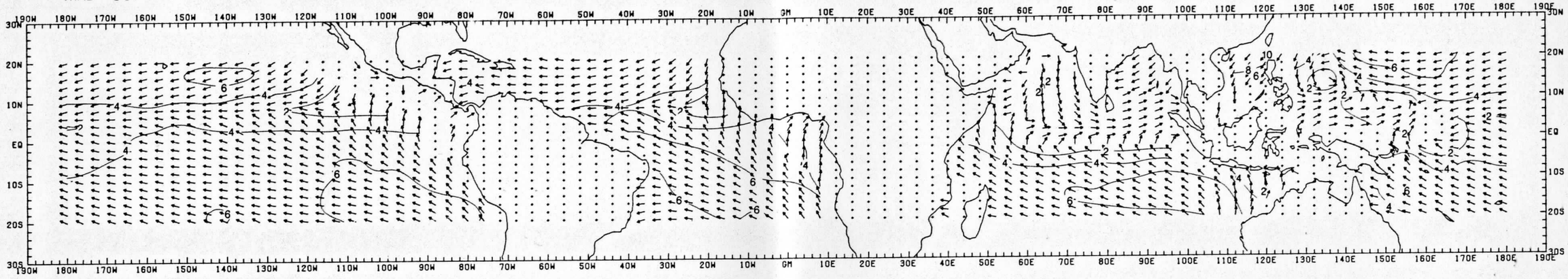

DIVERGENCE OCT 1979

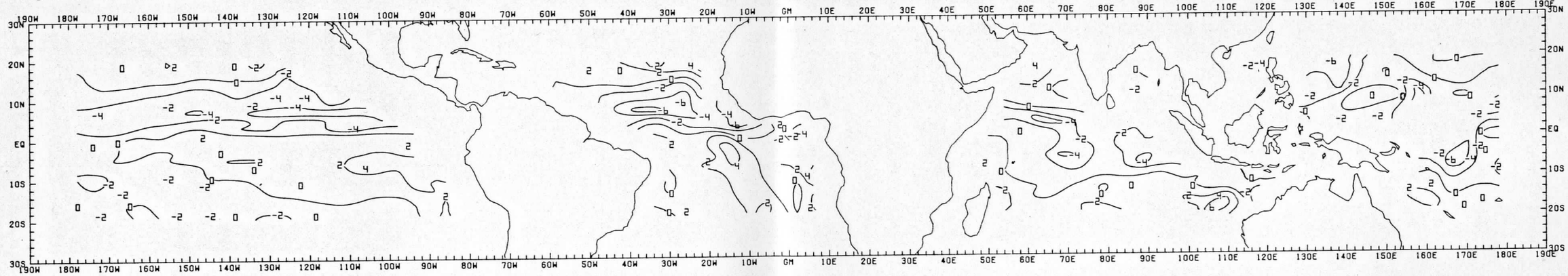

VORTICITY OCT 1979

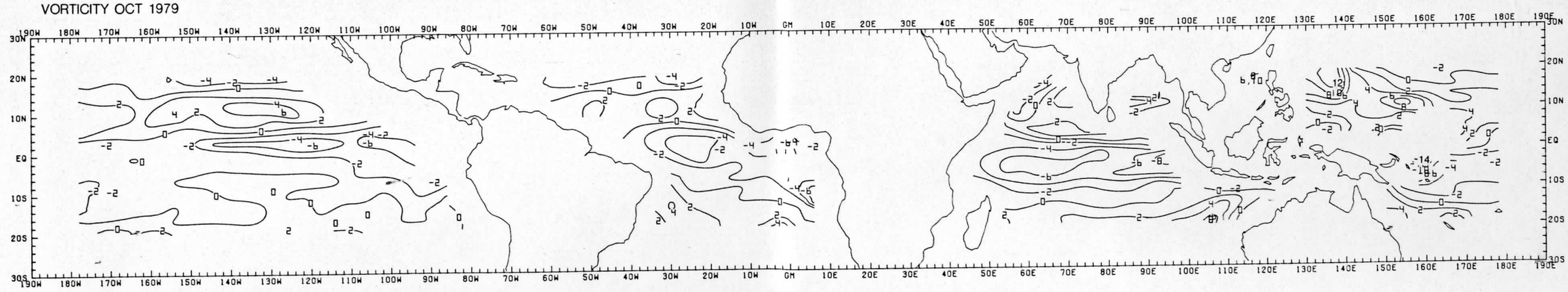

MEAN STRESS WINTER 1978/79

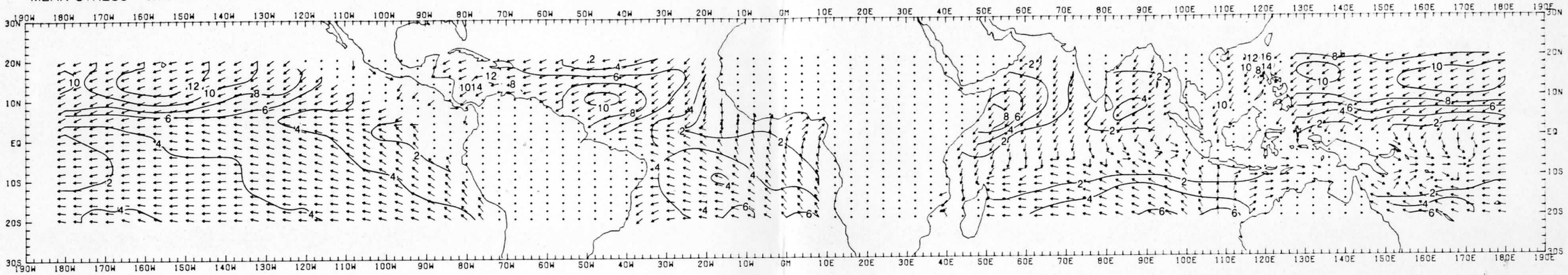

DIVERGENCE OF STRESS WINTER 1978/79

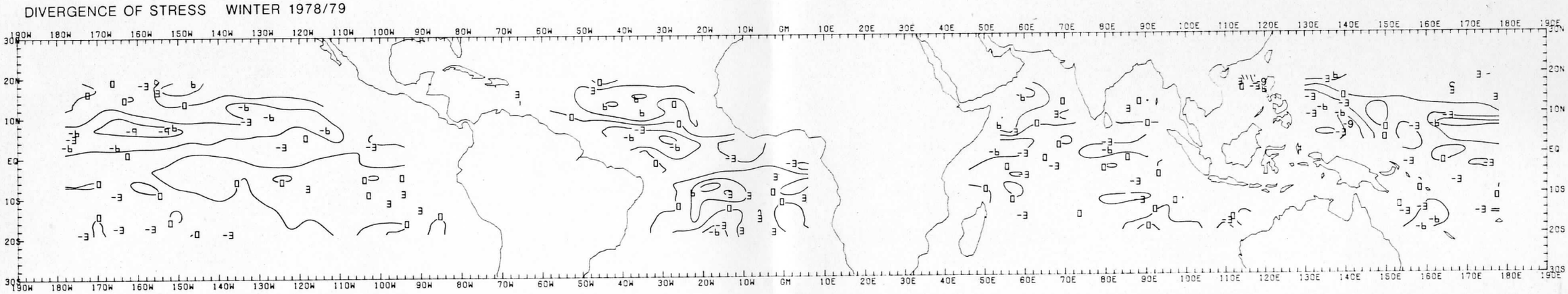

CURL OF STRESS WINTER 1978/79

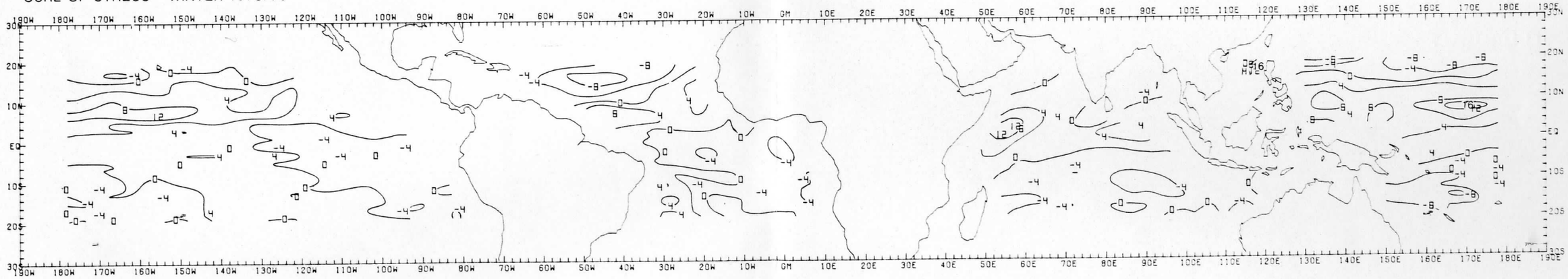

MEAN STRESS SPRIING 1979

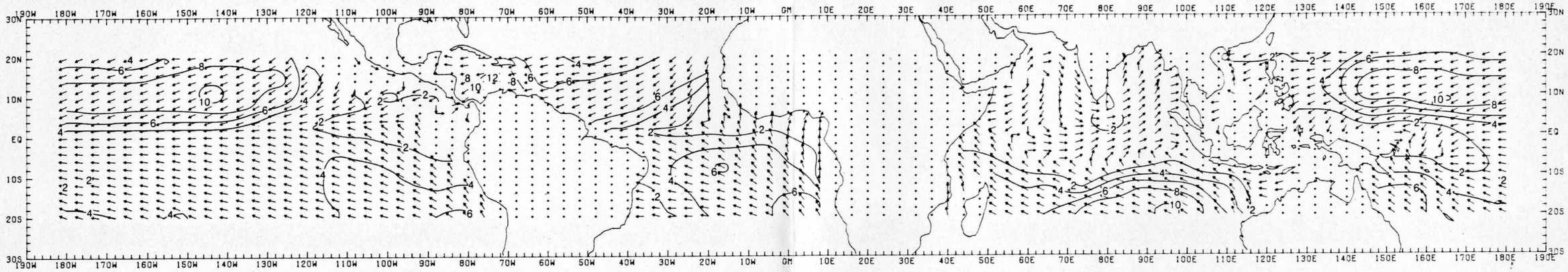

DIVERGENCE OF STRESS SPRING 1979

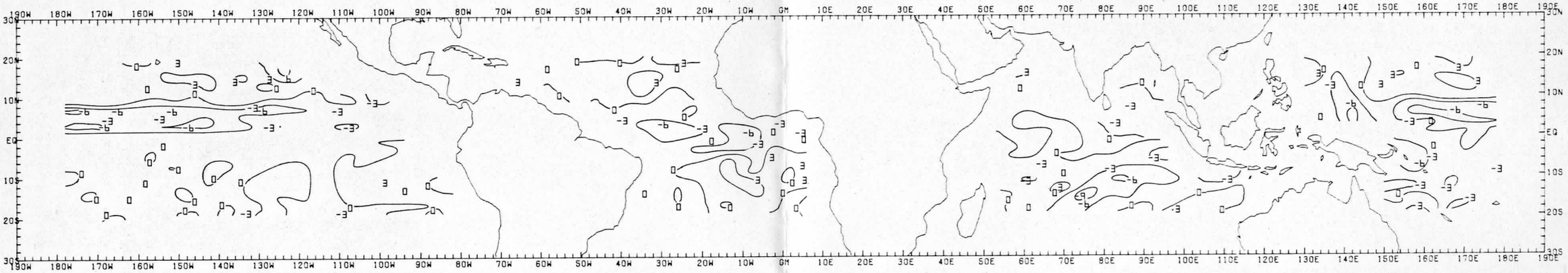

CURL OF STRESS SPRING 1979

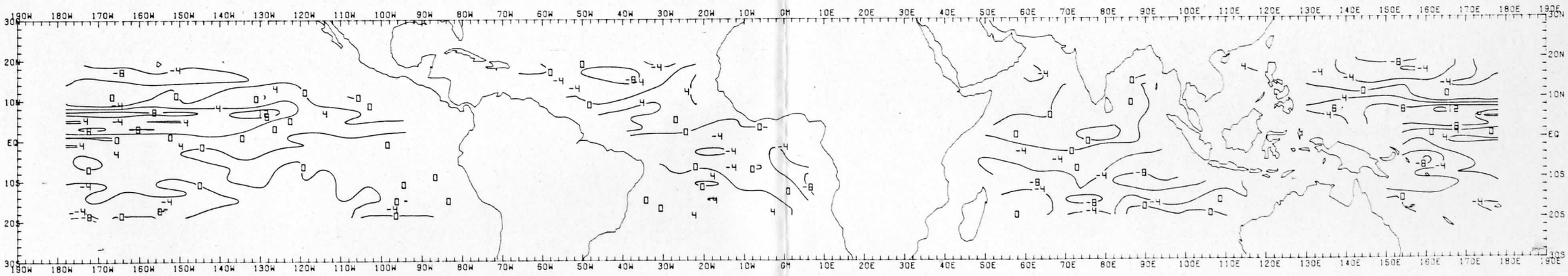

MEAN STRESS SUMMER 1979

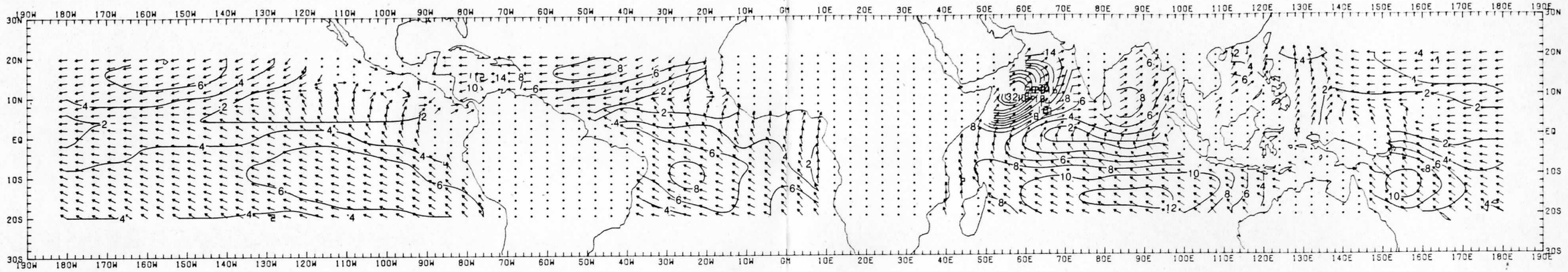

DIVERGENCE OF STRESS SUMMER 1979

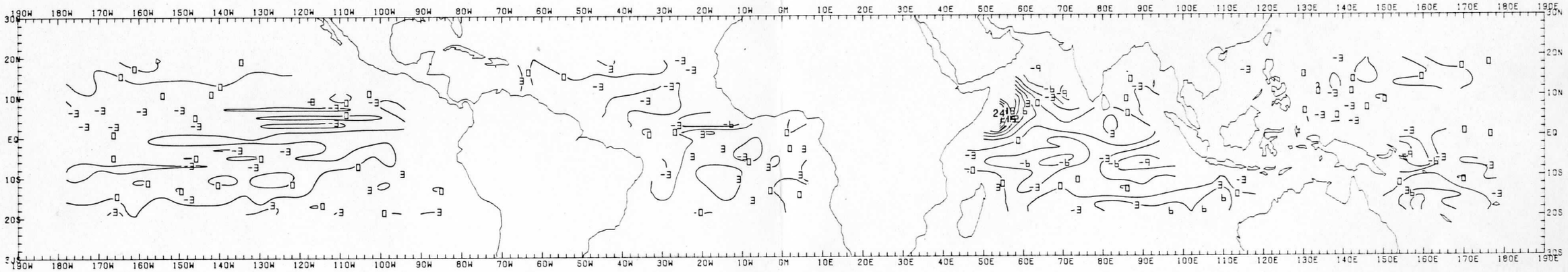

CURL OF STRESS SUMMER 1979

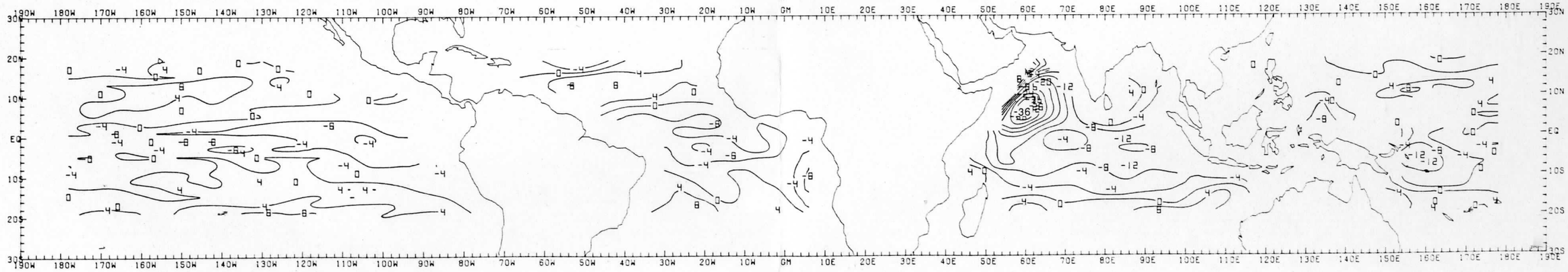

MEAN STRESS FALL 1979

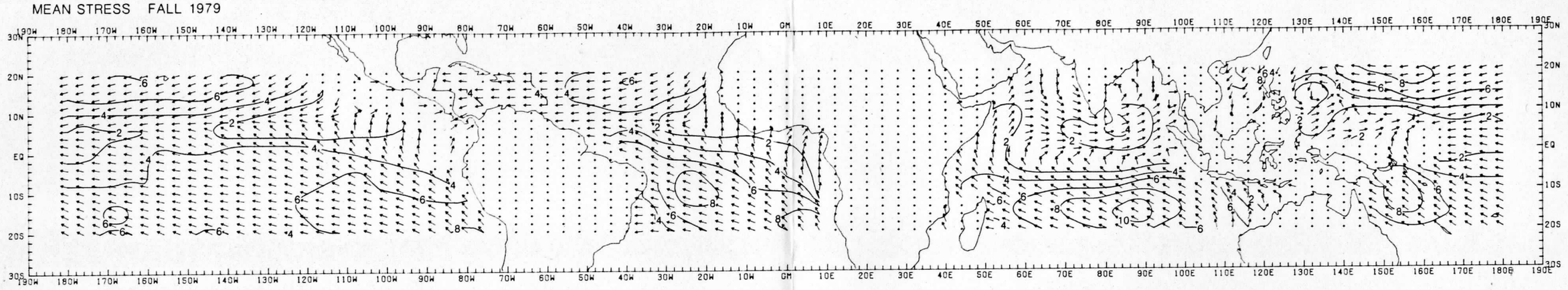

DIVERGENCE OF STRESS FALL 1979

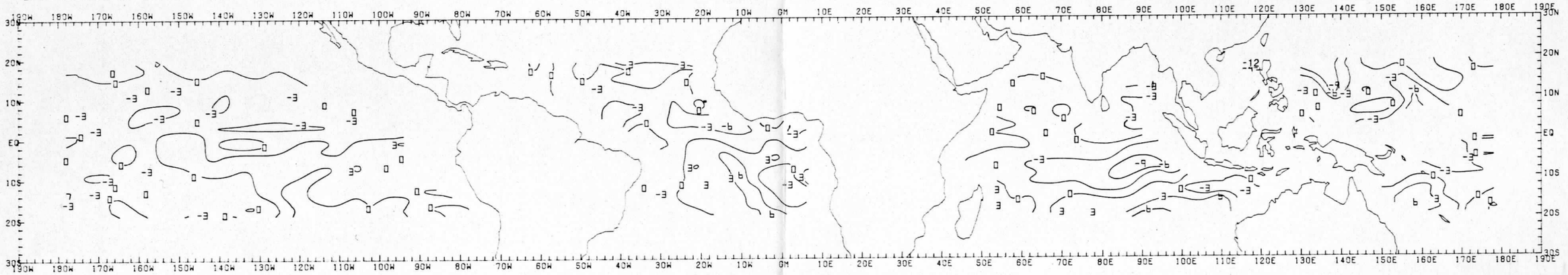

CURL OF STRESS FALL 1979

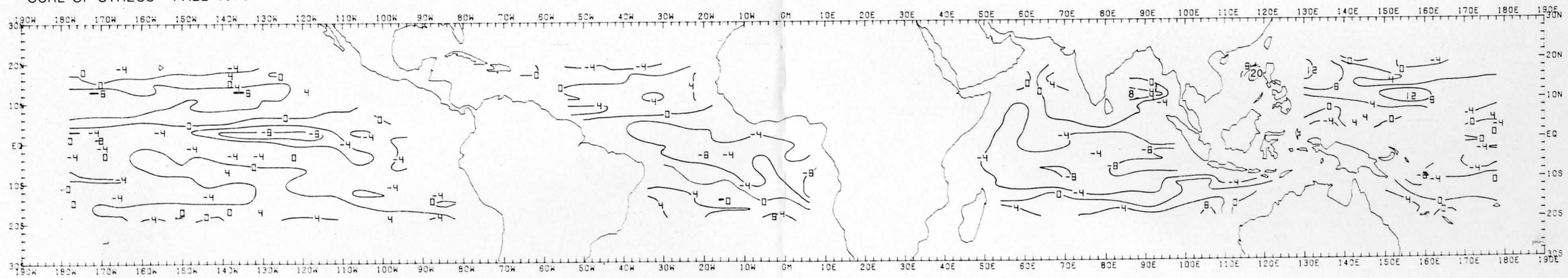

ANNUAL MEAN WIND 1979

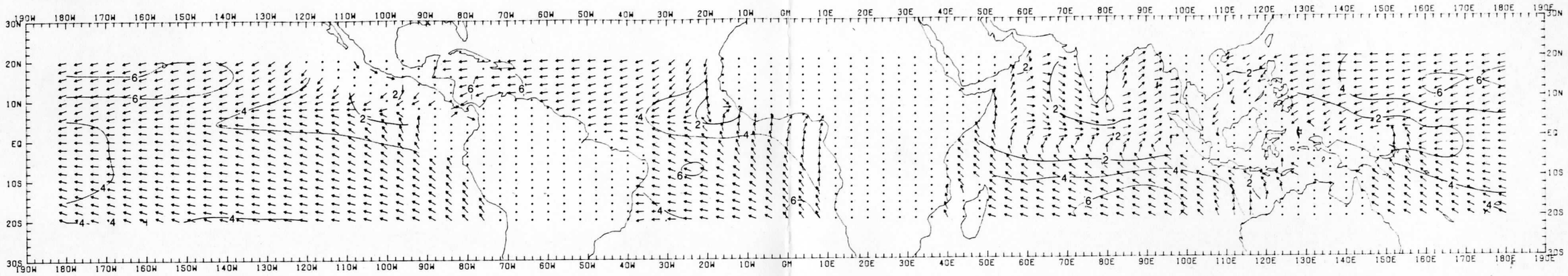

ANNUAL MEAN STRESS 1979

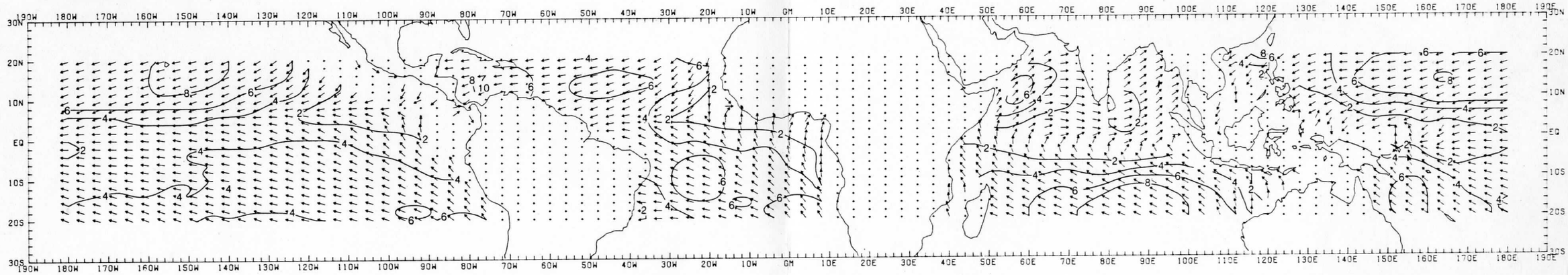

ANNUAL MEAN SCALAR STRESS 1979

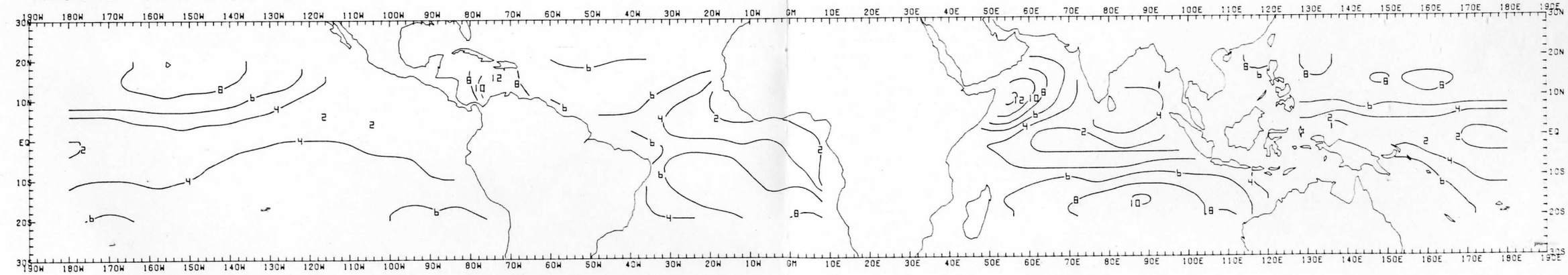

Appendix A: Comparisons with Other Sources

A.1. Discussion of Wind and Stress Patterns

The monthly stress fields composited from daily stress fields were presented in Charts 1-4. These plots will be discussed below and compared to Hellerman and Rosenstein (1983). Since the Hastenrath and Lamb (1977, 1979) climatologies and the Sadler et al. (1983) analysis present winds, not stress, we also present monthly surface wind analyses composited from daily analyses. Four months of wind analyses in the four seasons are shown in Charts 5-8. The surface wind field divergence and vorticity also are shown for the same months. Seasonal averages of stress, along with curl (vorticity) and divergence, are shown in Charts 9-12. An annual average surface wind field, vector stress field, and scalar stress field are shown in Chart 13.

It should be noted that the climatologies (Hellerman and Rosenstein; Hastenrath and Lamb) were compiled entirely from ship observations. Hellerman and Rosenstein present global stress for only two months, January and July, on a 6° latitude by 6° longitude grid. Hastenrath and Lamb present monthly wind fields on 2°x2° grids for all 12 months. Their climatologies are for the Atlantic, Indian Oceans, and a small part of the eastern Pacific Ocean adjacent to the Americas. They exclude the majority of the Pacific Ocean.

The Sadler et al. (1983) analysis is primarily for the Pacific Ocean, but includes a small part of the Caribbean adjacent to South America. Their analyses were made from cloud observations taken in 1979. There are three major differences from our analyses: 1) Sadler et al. use the NOAA/NESS and JMSC cloud motion data but not the Wisconsin data; 2) the cloud motions are transformed to surface level winds, using a climatological wind shear; and 3) ship data from the analysis period are not

directly input to the analysis. The Sadler et al. (1983) vertical shear climatology is derived from the difference between a seven-year climatology of NOAA/NESS and JMSC cloud motion data and a 30-year climatology of ship data. The vertical shear derived from the difference of two monthly averages was applied to the monthly averaged cloud motion analyses, not daily analyses as our algorithm was.

The discussion below centers on January, April, July, and October as representatives of the four seasons. Inspection of other months and the full year composite is encouraged, though they are given little attention here.

A.1.1 January 1979 -- The Pacific Ocean had two areas of strong easterly winds, one south of Hawaii (150°-170°W) and a second in the western north Pacific from 130°E to 150°E. The strongest winds were in December, which decreased into February. A small area of very intense northeasterly winds was found in the south China Sea near the Philippine Islands (120°E, 20°N) in December. This was part of the Asian winter monsoon, and our analysis depicted a 0.26 N/m^2 (12 m/s) average stress in December, which decreased to 0.08 N/m^2 (7 m/s) in February. Indication of the intense winter monsoon also can be found in the Hellerman and Rosenstein (1983) climatology. This depicted the strongest winds farther north, around 45°N latitude, beyond the range of our analysis.

For most of the Pacific, our wind anslysis resembles Sadler's. We depict maximum values of the northeasterly trades in the north Pacific to be slightly less than Sadler's. For example, Chart 5 shows maximum contours of 8 m/s south of Hawaii, while Sadler shows 9 m/s contours. However, our contour intervals are 2 m/s and the stress analysis (Chart 1)

shows small 0.12 N/m^2 contours equivalent to 8.8 m/s. The same is true in the western Pacific. The areas within these contours suggest we have analyzed the winds slightly lower than Sadler et al., but almost always within, 1 m/s of their analysis.

The divergence patterns calculated from the wind fields (Chart 5) are in general agreement with Sadler et al. The largest difference is in the Intertropical Convergence Zone (ITCZ, 5°-10°N latitude). We show $-4(10)^{-6}$ contours but Sadler et al. have $-6(10)^{-6}$. Our lower estimate probably results from our lower wind speeds.

The Hellerman and Rosenstein (1983) climatology depicts a slightly stronger wind stress in the Pacific than our analyses. A large area of 0.10 N/m^2 stress covers most of the north Pacific, while our FGGE analysis has areas of lighter winds from 150° to 170°W, with stresses as low as 0.04 N/m^2. Our south Pacific stress (0.04 N/m^2) for FGGE also was lighter than the Hellerman and Rosenstein climatology. However, since their contour intervals are 0.05 N/m^2, small variations are hard to find.

In the Atlantic we have reasonable agreement with the Hastenrath and Lamb climatology (1977). Highest winds were northeast of the Panamanian isthmus (76°W and 12°N). We found 0.12 N/m^2 (8.8 m/s) in December, decreasing in January to 0.08 N/m^2 (7 m/s), and increasing in February to 0.18 N/m^2 (10 m/s). Sadler et al. depict this maximum wind area on the eastern edge of their analysis with very similar values. Hastenrath and Lamb have a lower 9 m/s, maximum without large monthly changes.

Trade winds in the north Atlantic are similar to the climatology in pattern, but weaker. Our FGGE data have a maximum of 6 m/s. Hastenrath and Lamb give 8 m/s for the same area. The south Atlantic southeasterly trade winds are very close to the climatology, reaching about 6 m/s.

Hellerman and Rosenstein (1983) show higher stress estimates than our FGGE analysis. Their chart shows 0.10 N/m^2 over a large area of the north Atlantic, which we equate to 8 m/s -- a value similar to Hastenrath and Lamb (1977). In the south Atlantic, they have the same 0.10 N/m^2 value covering a much larger area, where we find only 0.04 to 0.06 N/m^2 in agreement with Hastenrath and Lamb. It appears Hellerman and Rosenstein have a higher drag coefficient than we used in the south Atlantic.

In the Indian Ocean, we see a strong northeasterly monsoon flow off the Asian continent. This attains a maxima of 6 m/s (0.08 N/m^2) along the east coast of Africa. This northeasterly wind is strongest in December, when a 0.10 N/m^2 stress (Chart 1) was found, which decreases in latter months. This is very similar to the Hastenrath and Lamb (1979) and Hellerman and Rosenstein (1983) climatologies.

The southern hemisphere easterly trade winds in the Indian Ocean peaked at 6 m/s or 0.06 N/m^2 in December (Chart 1) and decreased to 5 m/s (0.04 N/m^2) in later winter. The analyses resemble Hastenrath and Lamb's, but are less intense than Hellerman and Rosenstein's chart which shows 0.10 N/m^2 stresses where we have 0.06 N/m^2.

A.1.2. April 1979 -- The north Pacific trade winds decreased slightly from the winter season. Chart 6 depicts 6 m/s values over large areas. But because f the fine contour intervals, the stress analysis in Chart 2 indicates values 8-9 m/s are present corresponding to 0.10-0.12 N/m^2. Sadler's et al. analysis have slightly higher winds, reaching 10 m/s at 135°W and 11°N. The southeasterlies in the southern Pacific also are slightly lower in our estimate than theirs. Our divergence patterns (Chart 6) agree well.

Like January, the Atlantic FGGE analysis for April is similar to the Hastenrath and Lamb (1977) climatology. The intense trade winds in the Caribbean northeast of Panama were slightly stronger than the climatology, reaching 0.18 N/m^2 (10 m/s, Chart 2). This area, which also appeared in the Sadler et al. analysis, continued to fluctuate, with March and May mean values lower than April. The FGGE northeasterly trades in the north Atlantic were slightly weaker than the climatology, 6 m/s in Chart 6, while Hastenrath and Lamb have 8 m/s in that area. The southeasterlies in the south Atlantic agree with the climatological 6 m/s winds.

During April the Indian Ocean was in transition between the winter and summer monsoons. Anticyclonic air flow appeared in the Arabian Sea but with very light winds. This feature appeared in March (Chart 2) and anticyclonic vorticity also appeared in the Bay of Bengal. Hastenrath and Lamb (1979) show similar wind patterns. Easterly trade winds advanced northward and increased to 7 m/s, which is a climatological feature.

A.1.3. July 1979 -- The southeasterly trade winds in the southern Pacific increased in strength to 6 m/s on our analysis (Chart 7). Sadler depicts a slightly stronger 7 m/s. Relative to April, the northeasterly trades in the northern Pacific decreased slightly to 6 m/s in our analysis or 7 m/s in Sadler's. Southerly winds also appeared in the western Pacific (130°E) north of the equator where easterlies were previously present in both analyses.

Divergence patterns were similar in the two analyses. Sadler's analysis has larger values in the ITCZ reaching $-8(10)^{-6}$ s^{-1} where ours peaks at $-6(10)^{-6}$ s^{-1}. Two areas of intense convergence split by a weak area at 130°W appear in both analyses.

The Hellerman and Rosenstein (1983) climatology shows higher wind stress values for both hemispheres in the Pacific. We found 0.05 to 0.06 N/m^2 in the trades, whereas they show large areas in excess of 0.10 N/m^2.

The north Atlantic trade convergence line moved northward relative to its April position, and lighter winds extended westward toward the South American coast. The northeasterly trade winds were approximately 1 m/s lighter than the Hastenrath and Lamb (1977) climatology.

In the Caribbean, the small jet northeast of Panama mentioned in the January discussion was greater than 8 m/s on our July wind plot (Chart 7), while the stress plot (Chart 3) indicates 0.15 N/m^2 or 9 m/s. Sadler's analysis shows a small 10 m/s contour in this area. Hastenrath and Lamb (1977) indicate a 9 m/s jet for this month.

The south Atlantic southeasterlies were slightly weaker than the Hastenrath and Lamb charts, reaching only 6 m/s compared to 7 to 8 m/s in the climatology.

The Hellerman and Rosenstein (1983) climatology shows much stronger northeasterly trades than we found in the north Atlantic (0.15 N/m^2). Our FGGE analysis reaches only 0.05 N/m^2 outside of the Caribbean (Chart 3). The south Atlantic southeasterlies, however, are slightly stronger in our FGGE analysis (0.05 N/m^2) than the Hellerman and Rosenstein charts which show less than 0.05 N/m^2 stress over most of this area.

The Indian Ocean was dominated by the intense southwesterly jet in the Arabian Sea, which our FGGE analysis depicted at 12 m/s or 0.35 N/m^2 for the monthly average. This is slightly weaker than the Hastenrath and Lamb (1979) climatology, which displays the monthly average maximum wind as 15 m/s. It was also weaker than the Hellerman and Rosenstein (1983) climatology, which indicates a maximum averaged stress 0.40 N/m^2.

The southern Indian Ocean trade winds were weaker than both climatologies, reaching 8 m/s or 0.10 N/m^2 in our FGGE analysis. Hastenrath and Lamb (1979) report 9 to 10 m/s, and Hellerman and Rosenstein (1983) report 0.20 N/m^2.

A.1.4. October 1979 -- The strength of the south Pacific southeasterlies continued, 7 m/s (0.08 N/m^2) on our analysis and 8 m/s on Sadler et al. The north Pacific northeasterlies maintained small areas of 6 to 7 m/s. Our analysis was again slightly less than theirs. Our divergence patterns in the Pacific agree with Sadler et al., except near 100°W and 7°N where they depict an intense $-8(10)^{-6}$ s^{-1} value over a very small area. Our analysis has no wind data in this area because of the scarcity of ship reports and lack of a meaningful relationship between cloud and surface winds. A near constant divergence of $-4(10)^{-6}$ s^{-1} was found along the ITCZ.

The north Atlantic northeasterlies diminished in October, reaching only 4 to 6 m/s (0.06 N/m^2 on Chart 4). This is slightly weaker than the Hastenrath and Lamb climatology. The easterly jet in the Caribbean northeast of Panama subsided to 5-6 m/s both on our analysis and that of Sadler et al. This is only slightly stronger than Hastenrath and Lamb's 4 m/s. The south Atlantic southeasterlies were in agreement with Hastenrath and Lamb at 7 m/s.

The Indian Ocean had no strong Asian monsoon flow by October. Light winds were found from the equator northward. Light northeasterly winds present in the Bay of Bengal suggest the beginning of the winter monsoon. This deviates from the Hastenrath and Lamb (1979) climatology in which light southwesterly winds are depicted through October.

The southern Indian Ocean trade winds decreased in October to 6 m/s, slightly less than the Hastenrath and Lamb's.

A.2. Short Period Changes in the Asian Monsoon

The general pattern of the wind directions over the Indian Ocean was fairly steady during most of the months examined. To illustrate, vector average wind directions were compiled for two regions within the Indian Ocean. One was the area of the intense summer monsoon flow from the equator to 20°N which lies from 50°E to 60°E, plus the area from 10°N to 20°N between 60°and 70°E. The other region included the southern trade wind area from 10° to 20°S from 70° to 94°E (see Figure A.1). The daily average wind directions for each area are plotted in Figure A.2.

The trade winds blew from the southeast (90° to 130°) for the entire year of FGGE. Shifts to more easterly directions occurred during the northern spring, 1 March to 1 April (Julian day 60 to 91), and in the northern fall, 17 September to 2 October (days 260-275) and 16-26 November (days 320-330), followed by shifts back to the southeast.

In the Arabian Sea, the directions were more variable from December to April (days 335-91), when a shift from northeasterly to variable westerly and northwesterly winds occurred. On 9 June (day 160), the directions became very steady from the southwest. This persisted until the beginning of October (day 274) when they abruptly shifted back to the northeast.

The wind speeds exhibited large daily and weekly fluctuations (Figure A.2). A general decline in speed from February through April (days 30-120) in the Arabian Sea is evident with many oscillations. A slight increase in speed occurred at the beginning of May (day 121), followed by a strong speed increase on 12 June (day 163) when the Somali Jet reached its full

strength in the Arabian Sea. A relaxation in these winds occurred from 14 July to 26 July (day 195-207), followed by a second strong surge. The characteristically strong monsoon winds persisted through part of August and then declined starting on 23 August (day 235). A second low point was reached from 1-20 October (days 274-293). Subsequently speed increased in November (day 305) as the northwesterly winds of the second winter approached.

The trade winds displayed large speed oscillations at periods from 5 to 25 days with some small seasonal trends. From January through February, many changes in the trades occurred in synchronization with wind speed oscillations in the Arabian Sea. In April and May, when the Arabian Sea winds were weak and variable in direction, the trades remained strong, exhibiting two notable surges from 26 March to 8 April (days 85-98) and 28 April-6 May (days 118-126), with a lull between. When the Arabian Sea winds surged during the beginning of the summer monsoon, 15 July-3 July (days 166-184), the trades decreased in intensity for a short period. Later fluctuations in the trades were in phase with the monsoon, especially the monsoon break from 14-26 July (days 195-207). The trades surged as the monsoon winds declined, starting on 17 August (day 288). A spectral analysis of these time series over the full year indicated some correlation between the wind speeds in these two regions at periods from 13-20 days. But these correlations were very small because of large amplitude of the seasonal changes relative to the shorter period variations.

A.3. Comparisons to Past Monsoons

A study of the onset of 25 monsoons from 1934 to 1972 by Fieux and Stommel (1977) found the average starting date of monsoons to be 23 May.

The 1979 monsoon appeared to start around 5 May with light southwesterly winds, but did not surge to full strength until 12 June. Fieux and Stommel (1977) found 10 monsoons out of the 25 they studied to have multiple or extended starting periods. The latest extended to 8 June. This implies that the 1979 monsoon was unusually late in reaching full strength.

During June, July, and August, 1979, the monsoon was weaker than the climatology compiled by Bunker (see Bruce 1978). The wind stress computed by Bunker from ship data in the Arabian Sea (see Figure A.1, Marsden Squares 31, 66, and 67) ranged from 0.18 to 0.32 Nm^{-2} with an average of 0.26 Nm^{-2} for the three summer months. The FGGE data average 0.22 Nm^{-2} for the same months. Thus 1979 would rank among the seven weakest monsoons in Bruce's report.

A.4 Concluding Remarks

Generally the FGGE Year was similar to the Hastenrath and Lamb (1979) and Hellerman and Rosenstein (1983) climatologies. The main departure was the unusually late arrival of the Somali Jet in the Arabian Sea in mid June. This caused the May and June averaged winds in the Arabian Sea to be noticeably weaker than the climatology. The September and October mean winds indicate that the 1979 Asian summer monsoon ended early. Weaker southwesterly winds were found in the Arabian Sea in September, and a shift to northeasterly winds which was not in the climatology appeared in the Bay of Bengal in October.

Schott and Fernandez-Partagas (1981) made a wind analysis of parts of the FGGE year, using ship and some cloud motion data (but not the University of Wisconsin generated data). They found large variations in the Arabian Sea winds. Notable differences from our analysis were the area,

intensity, and location of the Somali Jet. Schott et al. report a 25 m/s jet from 18-20 June, somewhat stronger than presented here. Cloud motions from the Wisconsin analysis not corrected for sub-cloud shear (Young et al. 1980) reported similar winds, but our surface level combined ship and cloud motion analyses found a maximum of 18 m/s.

The Schott et al. analysis concentrates the Somali jet in a smaller area located about 250 km to the west of its position in the Wisconsin analysis for June. During the other periods studied by Schott et al. from January to July, our analyses were similar in speed, direction, and area of the winds east of the Somali coast.

The differences probably originate from the different data sets used or the relative emphasis given them. We made a separate analysis using only ship data, but with the same gridding procedures (not shown). This analysis located the jet to the west and reduced its area, more in agreement with Schott et al. However, we found negligible differences in the maximum speeds of the jet, when ship-only and combined ship-cloud analyses were compared. The ship reports in the Somali jet were highly variable. Most of the reports in excess of 25 m/s came from one ship. It appears that Schott et al. weighted these reports above the others. Our analysis weights ships only according to their distance from the grid point; otherwise, treating them equally. This weighting function diminished the extremely high reports and broadened the Somali jet somewhat.

There were many notable points of agreement with the wind analyses of Sadler et al. (1983) in the Pacific. Indeed, since we used similar data, cloud motions, agreement might be expected. However, our boundary layer wind shear corrections of the cloud motions were independently derived from theirs and based on a somewhat different strategy. We used more cloud

motion data and explicitly included the ship reports, which Sadler et al. does not appear to use directly in the analysis. These data, along with a different algorithm for correcting cloud motions for sub cloud shear, may account for Sadler's analyses being up to 1 m/s higher than ours in some places. The directional patterns were remarkably similar between our analysis and Sadlers.

Another point to consider is the disagreement between climatologies. Our wind analysis was close to the climatological wind analyses of Hastenrath and Lamb (1977, 1979), yet the Hellerman and Rosenstein (1983) stress climatology had mostly higher levels than ours. Both climatologies relied entirely on merchant ship data, so equivalent analyses would be expected. One evident cause of the differences between the climatologies is the drag coefficients used to estimate stress. Hellerman and Rosenstein (1983) used the formulation of Bunker (1976), while we used the formulation of Wu (1980). The Bunker (1976) formula considers thermal stability, while Wu (1980) does not. Also, Bunker's drag coefficients are 15-20% higher than Wu's for an air-sea temperature difference of 1°C and wind speeds under 8 m/s. This alone could account for a large part of this disagreement. Disagreement between climatologies and appropriate drag coefficient formulations are both important problems that need resolution. Future oceanographic programs will attempt wind stress measurements using spaceborne radars or passive microwave radiometers. The climatologies produced by these sensors will be compared to independently produced climatologies as one of several tests of their quality. We suggest ship-based climatologies need to be better understood before we compare them to new instrumentation.

In a recently completed report to NASA (Wylie and Hinton 1984), we showed that independent analyses of cloud motions and ship data for January and February 1979 differed by a random 1 m/s around a mean difference, or bias, of 1 m/s in the U component. This bias was expected because of sub-cloud shear. The same anlayses differed from NASA/Goddard Space Flight Center model analyses by 1.1 to 1.4 m/s random component. These comparisons indicate that the accuracy of wind analyses using these data is approximately 1 to 1.4 m/s. Granted, the combined cloud motion and ship product should be better than either alone, but is it significantly better than 1 m/s? Without other (independent) data, we cannot know. The goal of the World Ocean Circulation Experiment is a monthly accuracy of 0.25 m/s. More data from complementary sensors are required to reach this goal.

8/DW8/02.0

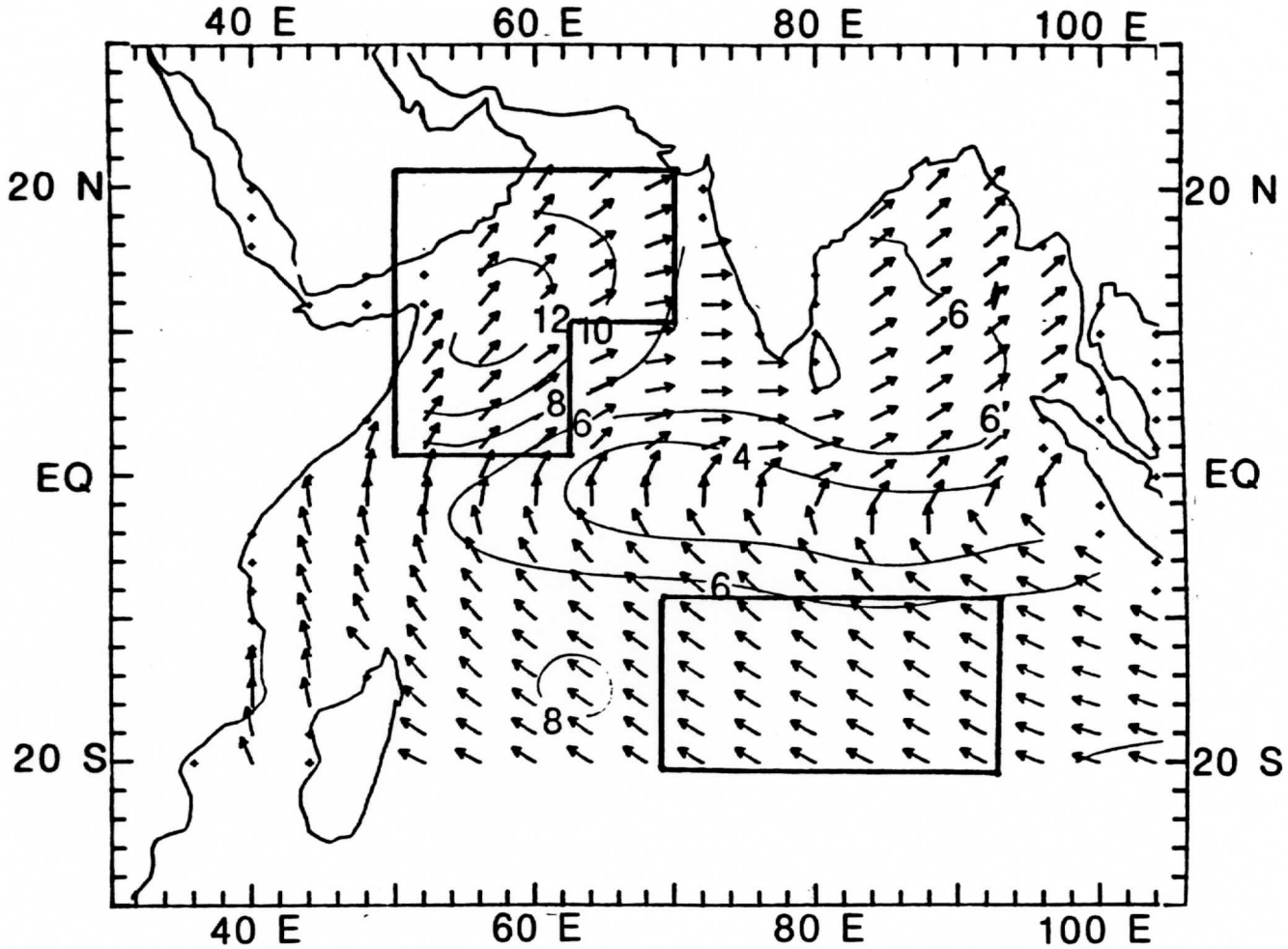

Figure A.1 The areas over which surface winds were averaged defined by the polygons. The Arabian Sea polygon corresponds to Marsden Squares 31, 66, and 67. (The winds shown are for July 1979 from Chart 7.)

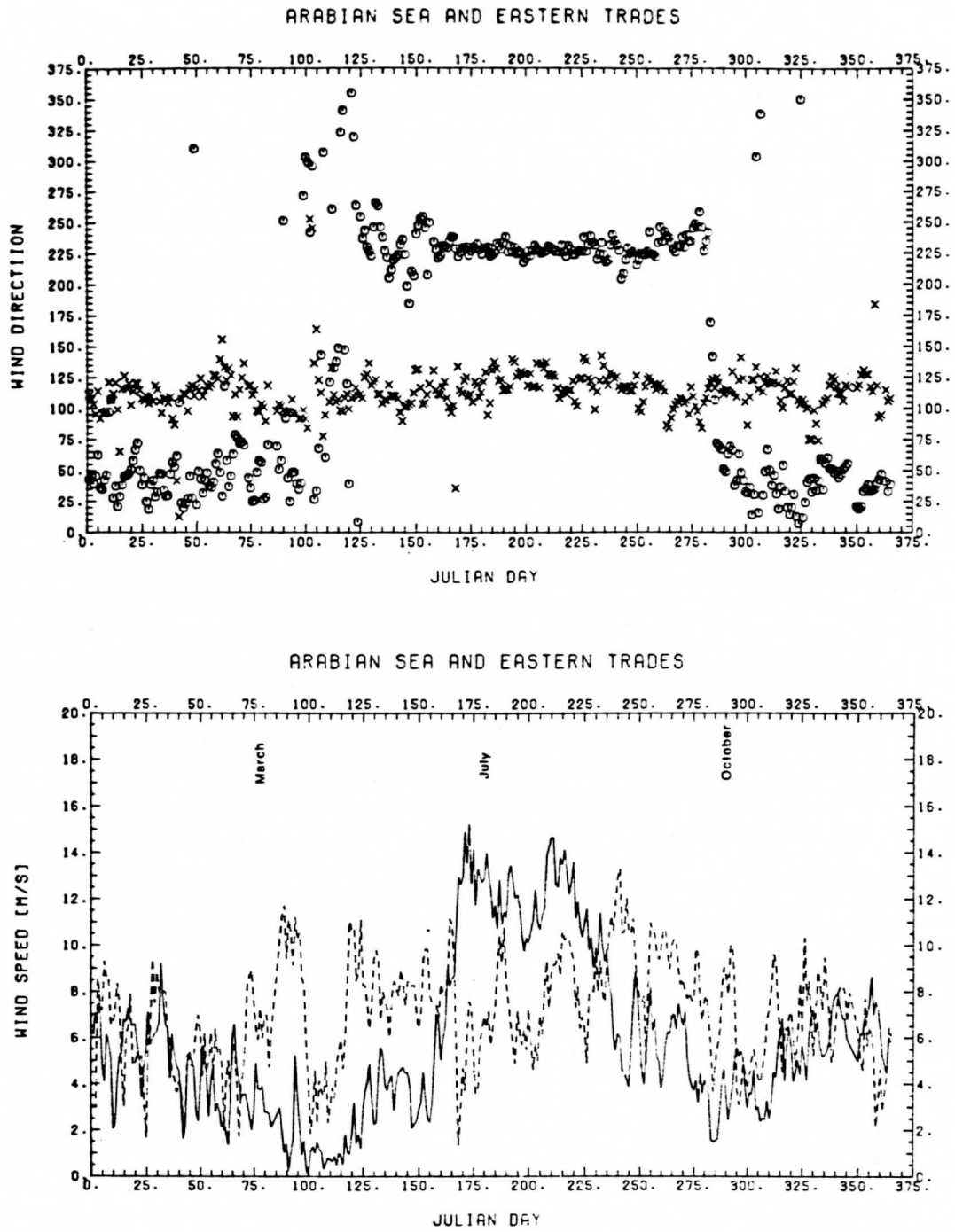

Figure A.2 The daily wind directions and speeds for the two polygons shown in Figure A.1 from 1 December 1978 (Julian Day 335) through 30 November 1979 (Julian Day 334). The Arabian Sea is denoted by the circles in the direction plot and the solid line in the speed plot. the trade winds are indicatd by X on the direction plot and the dashed line on the speed plot. The direction is the azimuthal angle from which the winds originated.

Appendix B: Regression Coefficients

Table B-1: Coefficients of the regressions used for transforming cloud level winds to surface level winds. The coefficients correspond to (3) in Section 4. Seasons are designated with a boreal bias: W is Dec-Feb, Sp is Mar-May, Su is June-Aug, and F is Sept-Nov. All values of C_4 have an implicit multiplier of 10^5. When a season is marked with an asterisk, the corresponding transformation is unsuitable for use.

Area No.	No. Hem. Season	Predicted Component	Const. C_0	U_c-Term. C_1	V_c-Term C_2	T_{a-2} Term C_3	f-term C_4
1	W	U_s	-0.54	0.53	0	-0.05	-2.90
		V_s	-0.58	0	0.53	-0.37	-0.87
	Sp	U_s	-1.7	0.52	0	0	0.0
		V_s	-1.7	0.08	0.47	-0.35	3.09
	Su	U_s	+0.48	0.55	0.04	0.12	-5.20
		V_s	+0.47	1.64	0.37	-0.06	0
	F	U_s	+1.24	0.57	0.03	0.07	-6.70
		V_s	0.23	0	0.56	0	-3.41
2	W	U_s	-0.36	0.43	0	0	0
		V_s	-0.52	0.21	0	-0.62	0
	Sp	U_s	+0.99	0.65	0	0	0
		V_s	-2.83	0	0.29	1.00	0
	Su	U_s	+1.20	0.50	0	0	0
		V_s	+3.24	0	0.41	0	-11.6
	F*	U_s	+1.79	0.48	0	0	0
		V_s	+7.80	0.16	0	0.60	-30.2

Area No.	No. Hem. Season	Predicted Component	Const. C_0	U_c-Term C_1	V_c-Term C_2	T_{a-s} Term C_3	f-Term C_4
3	W	U_s	-3.60	0.51	-0.07	0	3.82
		V_s	-3.10	0	0.43	-0.22	4.51
	Sp	U_s	-2.98	0.40	-0.11	-0.14	-0.84
		V_s	-2.35	0	0.48	-0.36	2.72
	Su	U_s	+0.43	0.50	-0.17	0.25	-7.03
		V_s	+1.26	-0.03	0.44	0	-6.93
	F	U_s	+0.20	0.59	-0.12	0	-3.86
		V_s	+0.64	0.04	0.50	0.11	-3.48
4	W	U_s	-2.90	0.31	-0.04	0	2.64
		V_s	-3.45	0	0.29	-0.31	3.71
	Sp	U_s	+0.56	0.50	-0.08	0	0
		V_s	-1.22	0.17	0.42	-0.27	5.04
	Su	U_s	+2.35	0.44	0	0.15	-1.44
		V_s	+0.20	0.08	0.59	-0.32	3.70
	F	U_s	+1.82	0.51	0.04	0	-2.93
		V_s	+0.19	0.17	0.59	-0.17	0

Area No.	No. Hem. Season	Predicted Component	Const. C_0	U_c-Term C_1	V_c-Term C_2	T_{a-s} Term C_3	f-Term C_4
5	W	U_s	-1.27	0.44	-0.05	0.24	-1.20
		V_s	+0.58	-0.06	0.50	-0.21	-5.50
	Sp	U_s	-1.29	0.44	-0.04	+0.08	0
		V_s	+1.17	0.13	0.42	-0.22	-7.54
	Su	U_s	-1.04	0.53	0	0.30	4.45
		V_s	+1.93	0.23	0.54	0	-1.91
	F	U_s	-0.97	0.57	0	0.34	5.62
		V_s	+1.23	0.11	0.62	0.24	-2.83
6	W*	U_s	+0.31	0.41	0	0	0
		V_s	+3.40	0	0	0	-25.5
	Sp*	U_s	-1.41	0.36	0	0.62	0
		V_s	+3.26	0.50	0	0	0
	Su*	U_s	-0.14	0	0	0	-30.64
		V_s	--	--	--	--	--
	F*	U_s	-0.20	0	0	0.74	24.68
		V_s	+4.39	0	0.23	0	0

Area No.	No. Hem. Season	Predicted Component	Const. C_0	U_c-Term C_1	V_c-Term C_2	T_{a-s} Term C_3	f-Term C_4
7	W	U_s	-2.69	0.30	0	0.12	0
		V_s	-0.19	-0.14	0.31	0	-22.23
	Sp	U_s	-2.40	0.32	0.08	0.19	2.30
		V_s	-0.66	-0.11	0.33	0.15	-18.89
	Su	U_s	-1.81	0.37	-0.12	0.21	5.92
		V_s	+2.94	0	0.23	0	-1.85
	F	U_s	-1.46	0.42	-0.14	0.17	5.83
		V_s	+4.19	0.25	0.29	0	-5.82
8	W*	U_s	+0.33	0.18	0	0	13.78
		V_s	+3.45	-0.11	0	-0.37	-12.10
	Sp	U_s	-0.91	0.11	0	0	12.02
		V_s	+3.63	0	0.08	0	-9.42
	Su*	U_s	-0.88	0.15	-0.05	0	13.47
		V_s	+4.22	0	0	0.42	2.12
	F*	U_s	-0.04	0.20	0	0	13.23
		V_s	+4.20	0	0	0	-5.80

Area No.	N.Hem. Season	Predicted Component	Const. C_0	U_c-Term C_1	V_c-Term C_2	T_{a-s} Term C_3	f-Term C_4
9	W	U_s	-1.13	0.32	0.08	0.29	-7.64
		V_s	-2.03	0.03	0.40	0.21	-7.28
	Sp	U_s	+0.13	0.51	0	0.13	1.74
		V_s	+0.02	0.03	0.66	0	-2.86
	Su	U_s	+1.39	0.28	0.05	0	20.69
		V_s	1.58	0.04	0.54	-0.13	-3.36
	F	U_s	0.87	0.37	-0.06	0.14	7.91
		V_s	1.09	0	0.51	-0.27	-3.86
10	W	U_s	-0.35	0.47	-0.04	0.19	4.07
		V_s	0.73	0	0.50	-0.05	-1.30
	Sp	U_s	-1.06	0.46	0	0.07	2.36
		V_s	0.44	0	0.55	0.13	-1.76
	Su	U_s	-1.89	0.53	0.06	0	0
		V_s	0.37	-0.06	0.43	0.49	-1.57
	F	U_s	-1.75	0.46	0.05	0	2.89
		V_s	1.29	0	0.54	0.26	0

Area No.	N.Hem. Season	Predicted Component	Const. C_0	U_c-Term C_1	V_c-Term C_2	T_{a-s} Term C_3	f-Term C_4
11	W	U_s	-2.28	0.39	0.07	-0.10	0
		V_s	2.18	0	0.47	0	2.22
	Sp	U_s	-2.12	0.39	0.07	-0.19	0
		V_s	0.98	-0.06	0.57	0	0
	Su	U_s	-2.26	0.49	0.09	-1.90	-1.43
		V_s	2.19	-0.09	0.45	0.22	3.26
	F	U_s	-1.84	0.57	0.13	-0.08	0
		V_s	2.01	0	0.60	0.18	2.16
12	W	U_s	0.88	0.48	-0.08	0.28	7.36
		V_s	-1.17	-0.09	0.53	0.22	-3.49
	Sp	U_s	0.88	0.50	0.09	0	6.86
		V_s	-0.09	-0.12	0.46	0.12	2.12
	Su	U_s	-0.58	0.48	0.08	-0.17	4.52
		V_s	2.27	-0.06	0.47	0.15	1.52
	F	U_s	-0.10	0.46	0	0	4.46
		V_s	0.53	-0.23	0.38	0.27	1.50

Area No.	N. Hem. Season	Predicted Component	Const. C_0	U_c-Term C_1	V_c-Term C_2	T_{a-s} Term C_3	f-Term C_4
13	W	U_s	-0.73	0.30	0	0	-7.54
		V_s	-1.90	0.23	0.46	0	0
	Sp	U_s	-1.22	0.48	0	0	0
		V_s	0.07	0	0.75	0	0
	Su	U_s	-0.41	0.64	0	0	0
		V_s	0.78	0	0.56	0	0
	F*	U_s	5.33	0	0	0	-16.49
		V_s	--	--	--	--	--
14	W	U_s	0.25	0.52	0	0	0
		V_s	-0.26	-0.15	0.60	0	-6.51
	Sp	U_s	-1.54	0.62	0	0	0
		V_s	1.12	0	0.55	0	0
	Su	U_s	-1.53	0.46	-0.27	0	0
		V_s	2.97	0	0.28	0	0
	F*	U_s	2.91	0	0	0	30.23
		V_s	--	--	--	--	--

Area No.	N. Hem. Season	Predicted Component	Const. C_0	U_c-Term C_1	V_c-Term C_2	T_{a-s} Term C_3	f-Term C_4
15	W	U_s	0.76	0.60	0	0	0
		V_s	-2.07	-0.08	0.48	0	-10.52
	Sp	U_s	1.32	0.48	0.15	-0.34	6.02
		V_s	-2.04	0	0.44	0.35	-9.92
	Su	U_s	-4.84	0.33	0.10	-0.23	-5.93
		V_s	2.32	0.12	0.41	0.60	0
	F	U_s	-1.67	0.56	0	0	5.26
		V_s	-1.15	-0.14	0.43	0.36	-8.00
16	W	U_s	-0.06	0.41	0	0	0
		V_s	-7.33	0	0.71	0	-18.55
	Sp	U_s	0.15	0.60	0	0	0
		V_s	0.81	0	0.92	0	0
	Su	U_s	-0.11	0.49	0	0	0
		V_s	2.08	0	0.51	0.50	0
	F*	U_s	-1.98	0	0.20	0	0
		V_s	1.32	0	0.87	0	0

References

Bruce, J.G., 1978: Spatial and temporal variation of the wind stress off the Somali coast. J. Geophys. Res. 83, 963-967.

Bunker, A.F., 1976: Computations of surface energy flux and annual air-sea interaction cycles of the north Atlantic Ocean. Mon. Wea. Rev. 101, 1122-1140, 1967.

Businger, J. and W. Seguin, 1977: Transports across the air-sea interface. Report of the U.S. GATE Central Program Workshop. 25 July - 12 August, National Center for Atmospheric Research, Boulder, CO, pp. 441-449.

Cadet, D. and G. Reverdin, 1981: The monsoon over the Indian Ocean during summer 1975. Part I: Mean fields. Mon. Wea. Rev. 109, 148-158.

Dunckel, M., L. Hasse, L. Krugermeyer, D. Schriever, and J. Wucknitz, 1974: Turbulent fluxes of momentum, heat, and water vapor in the atmospheric surface layer at sea during ATEX. Bound.-Layer Met. 6, 81-106.

Fein, J.S., and J. Kuettner, 1980: Report on the Summer MONEX field phase. Bull. Amer. Met. Soc. 5, 461-477, 1980.

Fieux, M. and H. Stommel, 1977: Onset of the southwest monsoon over the Arabian Sea from marine reports of surface winds: Structure and variability. Mon. Wea. Rev. 105, 231-236.

Garratt, J.R., 1977: Review of drag coefficients over oceans and continents. Mon. Wea. Rev. 105, 915-929.

Halpern, D. and R.A. Knox, 1983: Coherence between low-level cloud motion vectors and surface wind measurements near 0°, 152°W from April 1979 to February 1980. Atmosphere-Ocean 21, 82-93.

Hasler, A.F., W.C. Skillman, W.E. Shenk, and J. Steranka, 1979: In situ aircraft verification of the quality of satellite cloud winds over oceanic regions. J. Appl. Meteor. 18, 1481-1489.

Hastenrath, S., and P.J. Lamb, 1979: Climatic Atlas of the Indian Ocean. Part I: Surface Climate and Atmospheric Circulation. University of Wisconsin Press, Madison, WI 53706, 97 pp.

Hastenrath, S., and P.J. Lamb, 1977: Climatic Atlas of the Tropical Atlantic and Eastern Pacific Oceans. University of Wisconsin Press, Macison, WI 53706, 110 pp.

Hellerman, S. and M. Rosenstein, 1983: Normal monthly wind stress over the ocean with error estimates. J. Phy. Ocean. 13, 1093-1104.

Hubert, L.F. and L.F. Whitney Jr., 1971: Wind estimates from geostationary satellite pictures. Mon. Wea. Rev. 99, 665-672.

Hull, C.H. and N.H. Nie (eds.) 1981: SPSS Update 7-9. McGraw-Hill, New York, xxi, 402 pp.

ICAS, 1977: A United States Climate Program Plan, Committee on Atmosphere and Oceans, Federal Coordianting Council for Science, Engineering, and Technology, Washington, D.C. 20500.

Kondo, J., 1975: Air-sea bulk transfer coefficients in diabatic conditions. Bound.-Layer Met. 9, 91-112.

Mosher, F.R., 1979: Cloud drift winds from geostationary satellites. Atmospheric Technology, NCAR #10, 53-60.

Mosher, F.R., 1981: Compatibility of cloud tracked winds from United States, European, and Japanese geostationary satellites. Advances in Space Res. Vol 1, 139-146.

NAS, 1969: Plan for U.S. Participation in the Global Atmospheric Research Program, National Academy of Sciences, Washington, D.C.

NASA, 1980: Climate Observing System Studies: An Element of the NASA Climate Research Program, Workshop Report. First Climate Observing System Study Workshop, February 21-11, 1980, Goddard Space Flight Center, Greenbelt, MD 20771.

Pond, S., D.B. Fissel, and C.A. Paulson, 1974: A note on bulk aerodynamic coefficients for sensible heat and moisture fluxes. Bound.-Layer Met. 6, 333-339.

Sadler, J.C., B.J. Kilonsky, A.M. Hori, M.A. Lunden, and L.K. Oda, 1983: Surface winds, wind stress, and weather over the tropical Pacific during the FGGE Hawaii to Tahiti oceanographic shuttle. Univ. of Hawaii Dept. of Meteor. Rept. UHMET 83-01.

Schott, F. and Jose Fernandez-Partagas, 1981: The onset of the summer monsoon during the FGGE 1979 experiment off the east African coast: A comparison of wind data collected by different means. J. Geophy. Res. 86, 4173-4180.

Smith, S.D., 1980: Wind stress and heat flux over the ocean in gale force winds. J. Phy. Ocean. 10, 709-726.

Smith, S.D., 1981: Comment on "A new evaluation of the wind stress coefficient over water surfaces." J. Geophy. Res. 86, 4307.

Wu, J., 1980: Wind stress coefficients over sea surface near neutral conditions -- a revisit. J. Phy. Ocean. 10, 727-740.

Wylie, D.P., B.B. Hinton, and K.G. Millett, 1981: A comparison of three satellite based methods for estimating surface winds over oceans. J. Appl. Met. 10, 339-449.

Wylie, D.P. and B.B. Hinton, 1981: The feasibility of estimating large scale surface winds for the Summer MONEX using cloud motion and ship data. Bound.-Layer Met. 21, 357-368.

Wylie, D.P. and B.B. Hinton, 1982a: The wind stress patterns over the Indian Ocean during the summer monsoon of 1979. J. Phy. Ocean. 12, 189-199.

Wylie, D.P. and B.B. Hinton, 1982b: A comparison of cloud motion and ship wind observations over the Indian Ocean for the Year of FGGE. Bound.-Layer Met. 23, 197-208.

Wylie, D.P., B.B. Hinton, and M. Howland, 1983: Surface wind observations from cloud motions during FGGE. Tropical Ocean-Atmosphere Newsletter, Pub. by NOAA Pacific Marine Environmental Lab., Seattle WA, D. Halpern, editor, May No. 18, p. 2-4.

Wylie, D.P. and B.B. Hinton, 1984: A comparison of cloud motion and ship wind data to NASA/Goddard Space Flight Center General Circulation Model Analyses. Space Science and Engineering Center of the University of Wisconsin-Madison, Final Report for NASA Grant.

Young, J.A., H. Virji, D.P. Wylie, and C. Lo, 1980: Summer monsoon windsets from geostationary satellite data. Space Science and Engineering Center, University of Wisconsin-Madison, 127 pp.